Development of a Secure Underwater Sensor Suite for Real-Time Environmental Monitoring of Blue Carbon Ecosystems

by

Rudra Pratap Singh

A Thesis Submitted in Partial Fulfillment of the
Requirements for the Degree of

MASTER OF APPLIED SCIENCE

in the Department of Electrical and Computer Engineering

We acknowledge and respect the Lək^{w}əŋən (Songhees and X^{w}sepsəm/Esquimalt) Peoples on whose territory the university stands, and the Lək^{w}əŋən and W̱SÁNEĆ Peoples whose historical relationships with the land continue to this day.

Development of a Secure Underwater Sensor Suite for Real-Time Environmental Monitoring of Blue Carbon Ecosystems

by

Rudra Pratap Singh
B.Tech., Vellore Institute of Technology (Chennai, India), 2023

Supervisory Committee

Dr. Navneet Popli, Supervisor
(Department of Electrical and Computer Engineering)

Dr. Xiaodai Dong, Co-Supervisor
(Department of Electrical and Computer Engineering)

ABSTRACT

The health of Canada's blue-carbon ecosystems—kelp forests, seagrass meadows, and salt marshes—plays a vital role in marine biodiversity and long-term carbon sequestration. Yet these ecosystems are increasingly vulnerable to anthropogenic and natural stressors such as temperature variation, pH fluctuations, heavy-metal pollution, and hydrocarbon extraction. Traditional monitoring methods, relying on sporadic field sampling and manual analysis, fail to capture the temporal and spatial complexity of these changes. This thesis, Development of Machine Learning-Based Techniques for Monitoring and Analyzing the Effects of Natural and Manmade Stressors on Canada's Blue Carbon Ecosystem Using a Secure Underwater Communication Suite, presents a comprehensive hardware-driven approach to address these gaps. The research involves the design, fabrication, and laboratory validation of a modular underwater sensor suite deployed via a Blue Robotics ROV platform to collect high-resolution oceanographic data. The integrated system measures temperature, salinity, dissolved oxygen, pH, turbidity, and chlorophyll concentrations through a network of calibrated probes, ensuring precise and repeatable environmental sensing.

To support continuous operation, a secure underwater communication and data-handling framework was developed using a hybrid Ethernet-acoustic link and lightweight encryption protocols to preserve data integrity and mitigate cyber vulnerabilities within the Internet of Underwater Things (IoUT). Extensive laboratory testing in controlled aquatic environments demonstrated stable sensor calibration, minimal noise drift ($< 0.05\%$ FS), and consistent data throughput at depths up to 1 m. Complementary studies explored intrusion detection and federated-learning frameworks for distributed underwater nodes, strengthening the resilience of the proposed communication network.

The system enables near-real-time environmental monitoring and data synchronization between underwater nodes and surface control units. By combining reliable hardware sensing with secure data transport, the work advances Canada's capacity for sustained observation of blue-carbon habitats. The results contribute both an open hardware architecture for scalable underwater sensing and a validated communication protocol for secure marine data acquisition—foundations that can inform future autonomous monitoring networks and adaptive management strategies for coastal ecosystems.

Contents

List of Tables

List of Figures

ACKNOWLEDGMENTS

This research was made possible through the generous support of the National Research Council of Canada (NRC), whose funding enabled the development, experimentation, and validation of the methodologies presented in this thesis. Their contribution played a pivotal role in advancing the research objectives and realizing the outcomes of this work.

I would like to express my deepest gratitude to my supervisor, Dr. Navneet Kaur Popli, for her unwavering guidance, mentorship, and encouragement throughout my Master's studies at the University of Victoria. Her expertise in data-driven systems, thoughtful feedback, and steadfast support were invaluable in shaping the technical depth and clarity of this thesis.

My sincere appreciation also goes to my co-supervisor, Dr. Xiaodai Dong, for her insightful feedback, direction, and academic support throughout the course of this research. Her expertise in signal processing and communication systems greatly enhanced the rigor and coherence of this work.

I am also grateful to Dr. Mohammad Mamun from the National Research Council of Canada (NRC) for his technical insight, collaboration, and mentorship, particularly in the design and validation of the machine learning frameworks integrated into this research. His constructive guidance and collaborative approach significantly strengthened the practical and analytical quality of the study.

I extend my appreciation to Dr. Issa Traoré for his valuable guidance, support, and academic input during my program. His perspectives contributed meaningfully to my overall learning and development.

My heartfelt thanks go to my coauthors and colleagues — Bhan Singh, Manshaj Popli, Min Gu Kim, and all members of the SOLIDS Laboratory — for their partnership and contributions across the research papers forming the foundation of this thesis. Their shared dedication, technical discussions, and collaborative problem-solving made this journey both productive and rewarding.

I would also like to acknowledge the faculty and staff of the Department of Electrical and Computer Engineering at the University of Victoria for providing an excellent academic environment, research resources, and administrative support that were essential to the successful completion of my graduate studies.

Finally, I extend my heartfelt gratitude to my family, my sister Sneha Singh, and my friends for their constant love, patience, and belief in me. Their support

provided the motivation and resilience that sustained me through the many stages of this research.

Chapter 1

Introduction

1.1 Overview of Oceanographic Research and Blue Carbon Ecosystems

The world's oceans play a fundamental role in regulating the Earth's climate system and supporting biodiversity. Among the many coastal and marine habitats, blue-carbon ecosystems—including seagrass meadows, salt marshes, and kelp forests—are particularly vital because of their capacity to sequester and store atmospheric carbon dioxide. These habitats not only mitigate greenhouse-gas accumulation but also serve as nurseries for fish species, buffers against coastal erosion, and filters for pollutants [1, 2].

Canada, possessing the world's longest coastline, holds immense potential for conserving and managing blue-carbon reserves. However, these ecosystems face unprecedented threats from both natural and anthropogenic stressors, such as fluctuating water temperature, salinity variation, ocean acidification, hydrocarbon extraction, seismic exploration, and microplastic accumulation. The cumulative impact of these factors reduces habitat productivity and resilience [3, 4].

Traditional observation campaigns led by organizations such as Ocean Networks Canada (ONC) and the Department of Fisheries and Oceans (DFO) provide valuable insights but rely heavily on moored instruments and periodic field sampling. These approaches often lack the temporal resolution and spatial adaptability required to understand short-term variability or episodic stress events. Consequently, there is an urgent need for autonomous, high-resolution, and secure monitoring systems capable of collecting in-situ environmental data continuously

and relaying it to researchers in real time.

Recent advancements in robotics and sensor miniaturization have enabled compact underwater vehicles equipped with diverse environmental sensors. Yet, despite progress in mechanical and sensing technologies, major gaps persist in ensuring data integrity, communication security, and interoperability across distributed underwater networks [5, 6, 7]. The growing research field of the Internet of Underwater Things (IoUT) aims to interconnect these devices, but underwater environments impose unique physical and cybersecurity constraints that demand novel engineering solutions [8, 9].

1.2 Motivation for Underwater Sensor-Based Monitoring Systems

Conventional ocean-monitoring techniques, while scientifically valuable, are constrained by limited temporal resolution, operational costs, and dependence on human intervention. Field campaigns using research vessels provide snapshots of oceanic conditions, but temporal gaps between observations can obscure short-lived phenomena such as temperature spikes, salinity anomalies, or pollution events. Moored buoys, though capable of continuous measurement, are fixed in space and vulnerable to mechanical failure, biofouling, and vandalism.

To overcome these constraints, underwater robotic systems such as *Autonomous Underwater Vehicles (AUVs)* and *Remotely Operated Vehicles (ROVs)* have emerged as flexible platforms for environmental data collection. When equipped with modular sensor payloads, these vehicles can operate at various depths and locations, enabling adaptive and targeted data acquisition.

The motivation behind this thesis stems from the convergence of three fundamental needs in modern oceanographic research:

i. **Enhanced Data Availability and Accuracy:** Blue carbon studies require fine-scale, real-time environmental data to analyze stressor interactions. Existing techniques fail to deliver adequate temporal and spatial resolution.

ii. **Operational Modularity and Scalability:** There is a growing demand for sensor suites that are easily reconfigurable, allowing integration of new probes or data links without extensive hardware redesign.

To meet these needs, this work develops a **secure, modular, and real-time underwater sensor suite** built on the Blue Robotics ROV platform. The system incorporates temperature, pH, dissolved oxygen, oxidation-reduction potential (ORP), salinity, turbidity, chlorophyll, and depth sensors. These are controlled and logged via a Raspberry Pi 5 interface communicating through a tethered Ethernet link and an auxiliary acoustic channel for redundancy. The motivation is thus not only to improve the quality and reliability of data acquisition but also to strengthen the cyber-physical security of underwater monitoring systems.

1.3 Thesis Objectives and Research Questions

The overarching goal of this thesis is to design, develop, and validate a secure underwater sensing and communication platform that enables real-time monitoring of environmental parameters within blue carbon ecosystems. To accomplish this, the research was structured around four interrelated objectives that collectively address the hardware design, data security, analytical capacity, and practical deployment of the system.

1.3.1 Design and develop a modular sensor suite

The first objective is to **design and develop a modular underwater sensor suite** capable of capturing critical physical, chemical, and biological parameters in marine environments. The sensor suite forms the physical backbone of the monitoring system and was designed to balance reliability, scalability, and adaptability for different research missions.

The suite integrates multiple sensors including temperature (DS18B20), pH, dissolved oxygen, oxidation-reduction potential (ORP), salinity, turbidity, chlorophyll, and pressure sensors. Each sensor was carefully selected based on sensitivity, operating range, and long-term stability under submerged conditions. The system employs a **Blue Robotics ROV** as the carrier platform due to its open architecture and proven operational stability in coastal waters.

To ensure modularity, the sensor suite adopts a plug-and-play hardware configuration supported by standardized communication interfaces, including I^2C, UART, and analog channels. Each sensor is connected through dedicated waterproof bulkhead connectors and modular internal wiring harnesses, allowing individual

probes to be physically detached and replaced without disturbing the remaining system components.

At the firmware level, sensors are implemented as independent software modules with predefined communication addresses and configuration parameters. When a sensor is replaced, the corresponding module can be reinitialized and recalibrated through the software interface without requiring system-wide reconfiguration or recompilation. Power management circuits provide isolated and regulated supply rails to each sensor channel, preventing electrical interference and ensuring safe sensor replacement while the system is powered down.

A centralized processing unit based on the Raspberry Pi 5 coordinates data acquisition and sensor control across all modules. A Python-based firmware architecture manages real-time sampling, data logging, fault detection, and sensor health monitoring. This combined mechanical and software modularity enables rapid sensor replacement, calibration updates, and system reconfiguration in both laboratory and field environments.

The modularity of the design ensures that the system can be adapted for different environmental monitoring campaigns—from shallow coastal deployments to deeper benthic studies—without extensive redesign. In addition, this architecture provides a stable foundation for future integration of autonomous control algorithms and machine learning analytics.

1.3.2 Establish Secure Underwater Data Transmission

The second objective focuses on establishing a **secure and reliable underwater data transmission** framework. Communication in underwater environments is inherently challenging due to the rapid attenuation of electromagnetic waves, limited bandwidth, and multipath propagation effects. Traditional wireless methods such as Wi-Fi or radio frequency (RF) communication are ineffective underwater; therefore, this system integrates both **tethered Ethernet** and **acoustic communication channels**.

The tethered connection provides high-speed, low-latency communication for near-surface or short-range missions, enabling real-time sensor control and live data streaming. In contrast, the acoustic link serves as a redundant low-bandwidth channel that allows essential telemetry and alerts to be transmitted even when the tether is disconnected or signal conditions degrade.

To ensure the confidentiality and integrity of transmitted data, the system implements an encryption protocol compatible with lightweight communication constraints. Building on the federated learning framework developed in the associated IEEE Access 2025 publication, a hybrid encryption model was tested that combines symmetric encryption for bulk data and asymmetric key exchange for authentication. Checksum validation, timestamp synchronization, and onboard buffering mechanisms further safeguard data consistency and traceability.

The secure communication framework not only enhances trust in the collected data but also contributes to the broader goal of developing a resilient *Internet of Underwater Things (IoUT)* architecture for environmental monitoring applications.

1.3.3 Enable Real-Time Monitoring and Stressor Analysis

The third objective is to **enable real-time monitoring and stressor analysis** by deploying the developed hardware in field environments and integrating the data stream with analytical tools. This objective bridges the gap between hardware design and ecological application by transforming raw sensor measurements into meaningful environmental insights.

The deployed sensor suite collects continuous data on parameters such as temperature, salinity, dissolved oxygen, and pH—key indicators of marine ecosystem health. Real-time visualization software was developed to display live readings through a graphical interface, allowing operators to monitor sensor performance and environmental fluctuations during missions. Data collected during deployments in the Discovery Passage region were used to validate system functionality and generate temporal datasets for subsequent analysis.

These datasets form the empirical foundation for the analytical work described in later chapters, including the *Temporal Analysis of Oceanographic Data* (IEEE PACRIM 2024), which quantifies environmental variability across different time scales, and the *Federated Security Framework* (IEEE Access 2025), which demonstrates secure distributed data analysis.

Through continuous data collection and real-time feedback, the system provides early detection of anomalies such as rapid temperature shifts, oxygen depletion, or increased turbidity—conditions that can signify environmental stress events. This capability enhances the understanding of how natural and anthropogenic stressors influence blue carbon ecosystems and supports more effective

conservation and management strategies.

1.3.4 Research Questions

To guide the research process, the following questions were formulated:

RQ1. **How can a modular underwater hardware system be designed to achieve high accuracy, mechanical robustness, and long-term stability in varying oceanic conditions?** This question explores the engineering aspects of system reliability, focusing on materials, waterproofing, sensor calibration, and integration under the constraints of limited space and energy.

RQ2. **What communication architecture and encryption mechanisms are best suited for secure, low-latency data transmission in underwater environments?** The objective is to identify and validate communication strategies that maintain data integrity despite bandwidth limitations, multipath interference, and dynamic environmental factors.

RQ3. **How can real-time environmental data be leveraged to analyze the effects of natural and anthropogenic stressors on blue carbon ecosystems?** This question addresses how sensor-derived datasets can be used to detect patterns and correlations between stressors such as temperature changes, acidification, or pollution, and overall ecosystem health.

RQ4. **What system-level trade-offs exist between performance, security, and power consumption for long-duration underwater missions?** This question investigates optimization strategies for balancing communication security and computational complexity with limited onboard resources and battery capacity.

Together, these objectives and research questions define the technical scope of this thesis. They provide a structured pathway from mechanical design and communication reliability to secure data management and real-time environmental assessment, ensuring that the final system contributes both to engineering innovation and marine ecosystem conservation.

1.4 Scope and Limitations

The scope of this thesis encompasses the design, fabrication, and validation of a secure underwater sensor suite developed for the monitoring of environmental parameters within blue carbon ecosystems. The research integrates mechanical design, electronic systems, communication engineering, and software development into a cohesive framework capable of operating in near-shore and coastal waters. While the system is designed with versatility in mind, several operational boundaries and limitations are recognized in this phase of the work.

1.4.1 Scope of the Research

This research primarily focuses on the **hardware and system-level integration** necessary to support real-time underwater environmental monitoring. The thesis covers four major areas of development:

i. **Mechanical and Hardware Design:** Design and assembly of a modular sensor suite mounted on a Blue Robotics ROV platform. This includes the creation of waterproof housings, electrical harnessing, and sensor mounting mechanisms that can withstand moderate hydrostatic pressure conditions up to approximately 75 meters of depth.

ii. **Sensor Calibration and Data Acquisition:** Laboratory calibration of temperature, pH, dissolved oxygen, salinity, turbidity, and chlorophyll sensors to ensure data fidelity prior to field deployment. The scope also includes the implementation of firmware and a surface-based interface for real-time data acquisition and logging.

iii. **Field Validation and Data Analysis:** Testing and validation of the system were conducted in coastal waters near Discovery Passage, British Columbia. Data collected through these deployments were analyzed to evaluate system stability, accuracy, and responsiveness to environmental fluctuations.

The research is conducted within the framework of the *SOLIDS Lab* at the University of Victoria in collaboration with the *National Research Council Canada (NRC)*. While the thesis emphasizes engineering design, the resulting datasets also support broader environmental research by providing reliable, high-resolution data for machine learning and temporal analysis models.

1.4.2 Field Deployment and Environmental Conditions

Field trials were designed to test the functionality and robustness of the system under realistic marine conditions. Deployments were conducted primarily in shallow-to-moderate depth environments characterized by variable salinity, temperature, and turbidity. The chosen site provided an ideal testing ground for evaluating the effects of tidal fluctuations and current variations on sensor stability and data transmission reliability.

During deployments, the ROV was equipped with all primary sensors, onboard data logging modules, and the tethered communication interface. Environmental parameters measured included:

- Temperature and salinity variations due to tidal mixing.
- pH and dissolved oxygen fluctuations influenced by biological activity.
- Turbidity and chlorophyll concentration indicative of sediment resuspension and phytoplankton presence.

These measurements established a proof of concept for the system's ability to capture fine-scale, time-resolved oceanographic data critical to assessing ecosystem health. However, environmental factors such as strong currents, marine growth, and sediment interference imposed operational challenges that informed several system refinements.

1.4.3 Operational Limitations

While the developed system successfully achieved its intended objectives, it is important to recognize several limitations inherent to both the experimental design and environmental conditions:

1. **Depth and Pressure Constraints:** The system is designed for deployments at depths up to approximately 30 meters. Beyond this range, hydrostatic pressure may compromise sensor housings, connectors, or cable integrity. Future iterations will require enhanced pressure-resistant housings and mechanical reinforcements for deep-sea applications.

2. **Communication Bandwidth:** Underwater acoustic communication suffers from low data rates (typically less than 10 kbps) and susceptibility to multipath interference. While the tethered Ethernet link offers high-speed communication, its use limits operational mobility. As such, fully autonomous wireless operations are not yet implemented in this version of the system.

3. **Power Supply Duration:** The onboard power system, based on lithium-ion battery packs, enables continuous operation for approximately 3–4 hours. Long-term missions would require either battery-swapping strategies or external power tethers, which were not part of this study.

   Environmental Fouling and Calibration Drift: Extended submersion in marine environments leads to biofouling and sediment accumulation on sensor surfaces, which directly alters sensor response characteristics. Biological growth such as algae and microbial films can obstruct sensor membranes and optical paths, reducing mass transfer rates for electrochemical probes and attenuating signal intensity for optical sensors. Similarly, sediment deposition introduces additional scattering and absorption effects, particularly affecting turbidity and chlorophyll measurements.

   These physical obstructions modify the effective sensing interface between the probe and the surrounding water, resulting in changes to sensor sensitivity, increased response time, and gradual offset drift relative to initial calibration parameters. For electrochemical sensors (e.g., pH and dissolved oxygen), fouling alters diffusion gradients across the sensing membrane, while for optical sensors it reduces light transmission efficiency and increases background noise. As a consequence, calibration coefficients derived under clean laboratory conditions may no longer accurately represent in-situ sensor behavior during prolonged deployments.

   To mitigate these effects, regular sensor cleaning and recalibration are necessary to restore measurement fidelity and maintain long-term reliability. Although antifouling strategies such as mechanical wipers, copper-based coatings, or ultraviolet sterilization have been reported in the literature, the integration of automated antifouling systems was beyond the scope of this research and is identified as a priority for future system enhancements.

4. **Security Evaluation:** While encryption protocols were tested in laboratory

simulations, real-world penetration testing under dynamic underwater conditions remains pending. Comprehensive validation of the security framework against targeted attacks such as spoofing, flooding, or DDoS simulations will be conducted in future extensions.

5. **Environmental Coverage and Sampling Density:** Data were collected over limited spatial and temporal scales. The relatively small deployment area restricts extrapolation of results to larger ecosystems without additional validation.

6. **Mechanical Handling and Stability:** Operating the ROV in strong tidal currents occasionally affected platform stability, resulting in short-term fluctuations in sensor orientation and data noise. These effects were mitigated through post-processing filters and outlier rejection methods.

1.4.4 Assumptions and Constraints

Several assumptions underlie the scope of this research:

- Environmental variables such as salinity and temperature gradients are assumed to remain approximately homogeneous over small spatial scales during short-term missions.
- Sensor calibration performed in laboratory conditions is assumed to remain valid throughout short-duration field trials.
- The acoustic communication link is assumed to operate under line-of-sight conditions within a 50–70 meter range for telemetry transmission.

These assumptions enabled the construction of a controlled yet realistic framework for system design and testing. Future work should aim to validate these assumptions under diverse field conditions, including variable depths, extended mission durations, and more complex environmental dynamics.

1.5 Contributions

This thesis makes significant contributions to the development of secure, modular, and real-time underwater monitoring systems for environmental and oceano-

graphic research. The outcomes of this work advance both the engineering foundations of underwater sensing and the analytical frameworks used to interpret complex ocean datasets. The research integrates contributions from hardware design, software development, data security, and analytical modelling, validated through experimental deployments and peer-reviewed publications.

1.5.1 Hardware Architecture for Modular Underwater Sensing

The first major contribution of this work is the design and implementation of a **modular underwater sensor suite** capable of performing multi-parameter environmental monitoring. The system architecture emphasizes flexibility, robustness, and ease of reconfiguration, allowing the integration of diverse sensors for various deployment scenarios.

- The sensor suite incorporates temperature, pH, dissolved oxygen, oxidation–reduction potential (ORP), salinity, turbidity, chlorophyll, and pressure sensors. These sensors were selected and calibrated to address the principal physical and chemical parameters influencing blue-carbon ecosystem health.
- A central control unit based on a Raspberry Pi 5 microcomputer coordinates data acquisition, time-stamping, and logging. Peripheral sensor modules communicate through a combination of I^2C, UART, and analog interfaces, allowing for efficient signal routing and synchronized sampling.
- A custom power-management subsystem regulates voltage and current distribution from onboard lithium-ion battery packs, enabling 3–4 hours of continuous operation. The design includes modular connectors, waterproof housings, and cable glands rated to 30 m depth, ensuring mechanical reliability under hydrostatic pressure.
- The hardware assembly is integrated onto a Blue Robotics ROV chassis, chosen for its open-source compatibility and modular payload capacity. The platform allows for easy reconfiguration between surface-tethered and semi-autonomous missions.
- A Python-based interface manages sensor polling and live visualization at the surface station, enabling real-time feedback during deployment and simplifying post-processing workflows.

This modular architecture represents a practical, field-deployable solution to the challenges of long-term marine environmental observation. It provides a scalable foundation for future multi-node underwater networks and supports the continuous acquisition of high-resolution data essential for environmental modelling and ecosystem assessment.

1.5.2 Secure Communication Protocol Design

The second core contribution involves the creation of a **secure underwater communication framework** that ensures data integrity, confidentiality, and resilience within constrained bandwidth environments. Given the vulnerabilities associated with the emerging Internet of Underwater Things (IoUT), this research addresses cybersecurity as an intrinsic component of system design rather than a post-deployment addition.

- A hybrid communication structure was implemented, combining a high-speed tethered Ethernet link for surface-level operations and an acoustic telemetry link for redundancy in untethered or degraded conditions.
- To safeguard data transmitted through these channels, a **lightweight encryption protocol** was developed that employs symmetric encryption for sensor data packets and asymmetric key exchange for device authentication. This protocol was tested for latency, throughput, and packet-loss resilience under varying network loads.
- The security framework builds upon the federated learning-based intrusion detection methodology described in the author's IEEE Access 2025 publication. This integration enables distributed validation of network behavior and anomaly detection across multiple underwater nodes without centralizing sensitive data.
- Additional mechanisms, including checksum validation, timestamp verification, and data-integrity hashing, were implemented to prevent packet corruption and spoofing. Together, these features establish a secure data pipeline that maintains synchronization between underwater devices and the surface control unit.

This contribution strengthens the reliability and trustworthiness of underwater monitoring infrastructures and establishes a blueprint for future IoUT security standards. By integrating cybersecurity directly into the hardware and firmware layers, the system mitigates one of the most critical bottlenecks in deploying large-scale, real-time ocean sensor networks.

1.5.3 Integration of Analysis Frameworks from Published Works

The third contribution extends beyond hardware and security to the **integration of advanced analytical frameworks** derived from the author's peer-reviewed publications. These frameworks transform the raw data acquired by the underwater sensor suite into meaningful insights about environmental variability, stressor interactions, and network vulnerability.

i. **Temporal Analysis of Oceanographic Data (IEEE PACRIM 2024):** The datasets collected by the developed sensor system were used to study temporal fluctuations in temperature, salinity, and dissolved-oxygen levels in coastal British Columbia. The analysis introduced signal-processing and visualization techniques for trend identification and anomaly detection in oceanographic time series.

ii. **Federated Security Framework (IEEE Access 2025):** The secure underwater network data served as a testbed for a federated learning-based intrusion-detection model. This model demonstrated that distributed learning can effectively identify cyber threats within underwater communication networks while preserving data privacy and minimizing transmission overhead.

iii. **IoUT DDoS Detection and Prediction (Submitted 2025):** The hardware platform provided validated network-traffic datasets used to train and evaluate machine-learning models—Decision Trees, SVM, K-Nearest Neighbours, AdaBoost, and Random Forest—for DDoS detection in underwater communication systems. Experimental results achieved up to 99 % classification accuracy under base conditions and 96 % under high-load scenarios at 1 m depth.

These analytical contributions bridge the gap between raw sensor data and actionable information for environmental management and cybersecurity. Together,

they illustrate how integrated sensing and analytics can advance both ecological monitoring and network resilience within marine systems.

Collectively, these contributions establish a unified framework for secure, autonomous, and data-driven monitoring of blue-carbon ecosystems. The research not only advances underwater instrumentation and network security but also provides a scalable foundation for future interdisciplinary studies in marine environmental management.

Publications

The contributions of this study have been disseminated through the following peer-reviewed publications and conference proceedings:

1. R. P. Singh, B. Singh, and N. K. Popli, "Temporal Analysis of Oceanographic Data: Insights into Environmental Variability and Trends," *2024 IEEE Pacific Rim Conference on Communications, Computers and Signal Processing (PACRIM)*, Victoria, BC, Canada, 2024, pp. 1–9.
   DOI: 10.1109/PACRIM61180.2024.10690219.
   Keywords: Temperature sensors, Statistical analysis, Oceanography, Environmental data visualization, Marine ecosystems.

2. M. Singh Popli, R. P. Singh, N. Kaur Popli, and M. Mamun, "A Federated Learning Framework for Enhanced Data Security and Cyber Intrusion Detection in Distributed Networks of Underwater Drones," *IEEE Access*, vol. 13, pp. 12634–12646, 2025. DOI: 10.1109/ACCESS.2025.3530499.
   Keywords: Internet of Underwater Things (IoUT), Federated learning, Cybersecurity, Intrusion detection, Underwater drones.

3. M. Gu Kim, Q. Luo, R. P. Singh, N. Kaur Popli, and M. Mamun, "Enhancing Underwater Network Security: ML-Based Detection and Prediction of DDoS Attacks in IoUT Networks," *IEEE Access*, vol. 13, pp. 190618–190629, 2025. DOI: 10.1109/ACCESS.2025.3621594.
   Keywords: Machine learning, Underwater communication, Cybersecurity, IoUT, DDoS attack detection.

4. R. P. Singh, N. K. Popli, and M. Mamun, "Design and Validation of a Modular Underwater Sensor Suite for Autonomous Environmental Monitoring,"

(manuscript in preparation, 2025).

This paper presents the hardware, communication, and power-optimization components of the system developed as part of this thesis. It details the modular sensing architecture, low-power design, hybrid Ethernet–acoustic telemetry, and in-situ validation for scalable and secure marine observation systems.

Chapter 2

Literature Review

2.1 Introduction

Monitoring and preserving marine ecosystems have become central to contemporary oceanographic research. Among these ecosystems, *blue carbon* environments such as seagrass meadows, mangroves, salt marshes, and kelp forests play a pivotal role in global carbon sequestration. They act as natural carbon sinks, storing atmospheric CO_2 in sediments and biomass. However, these ecosystems are increasingly affected by natural and anthropogenic stressors, including temperature anomalies, pH fluctuations, eutrophication, hydrocarbon contamination, and plastic pollution [10, 11, 12, 13]. Reliable, high-frequency data acquisition is thus critical for understanding and mitigating these impacts.

Traditional oceanographic monitoring methods—based on ship-based sampling, moored buoys, and fixed observatories—offer valuable but limited insights. Their spatial coverage is sparse, temporal resolution intermittent, and maintenance costly [14, 15]. In contrast, the past decade has seen the rapid emergence of autonomous underwater systems, mobile sensor suites, and Internet of Underwater Things (IoUT) networks, enabling real-time data collection at unprecedented resolution. Integrating secure, modular sensing platforms with autonomous vehicles has become an essential frontier for marine environmental monitoring [16, 17, 18].

This chapter synthesizes the scientific and engineering progress underlying such systems. It reviews research in four main domains that underpin the present thesis:

1. Modular underwater sensor hardware and calibration frameworks;

2. Underwater communication technologies and acoustic-optical hybrid models;

3. Security, intrusion detection, and federated learning frameworks in IoUT networks; and

4. Blue-carbon ecosystem monitoring applications and policy relevance.

Together, these strands provide the foundation for the secure, real-time monitoring system developed in this research.

2.2 Blue Carbon Ecosystems and Data-Monitoring Challenges

Blue-carbon ecosystems are globally recognized as efficient long-term carbon sinks. Fourqurean *et al.* [10] demonstrated that seagrass meadows store carbon at rates comparable to tropical forests, while Macreadie *et al.* [11] emphasized their vulnerability to temperature and nutrient stress. Serrano *et al.* [12] quantified carbon burial and degradation rates under anthropogenic disturbance. These studies underline that short-term physical and biochemical variability—temperature spikes, hypoxic events, diel pH cycles—strongly modulate carbon fluxes. Capturing such variability requires continuous, multi-parameter observations.

Global observing programs such as Ocean Networks Canada (ONC), the European Multidisciplinary Seafloor Observatory (EMSO), and Japan's JAMSTEC maintain cabled nodes for long-term monitoring, yet their infrastructure remains fixed and costly to extend. Bertram *et al.* [13] highlight the trade-off between spatial density and temporal resolution in these networks. The need for adaptable, low-cost, mobile platforms—ROVs, AUVs, and moored modular systems—has therefore intensified. Figure 2.1 illustrates this concept of blue-carbon monitoring.

Autonomous sensor platforms bridge the gap between regional observatories and process studies. By coupling mechanical mobility with real-time sensing, they can map gradients in dissolved oxygen, temperature, and turbidity across estuaries and coastal habitats. However, effective deployment demands progress in three dimensions: robust hardware design, reliable underwater communication, and secure data integrity—a triad explored in the following sections.

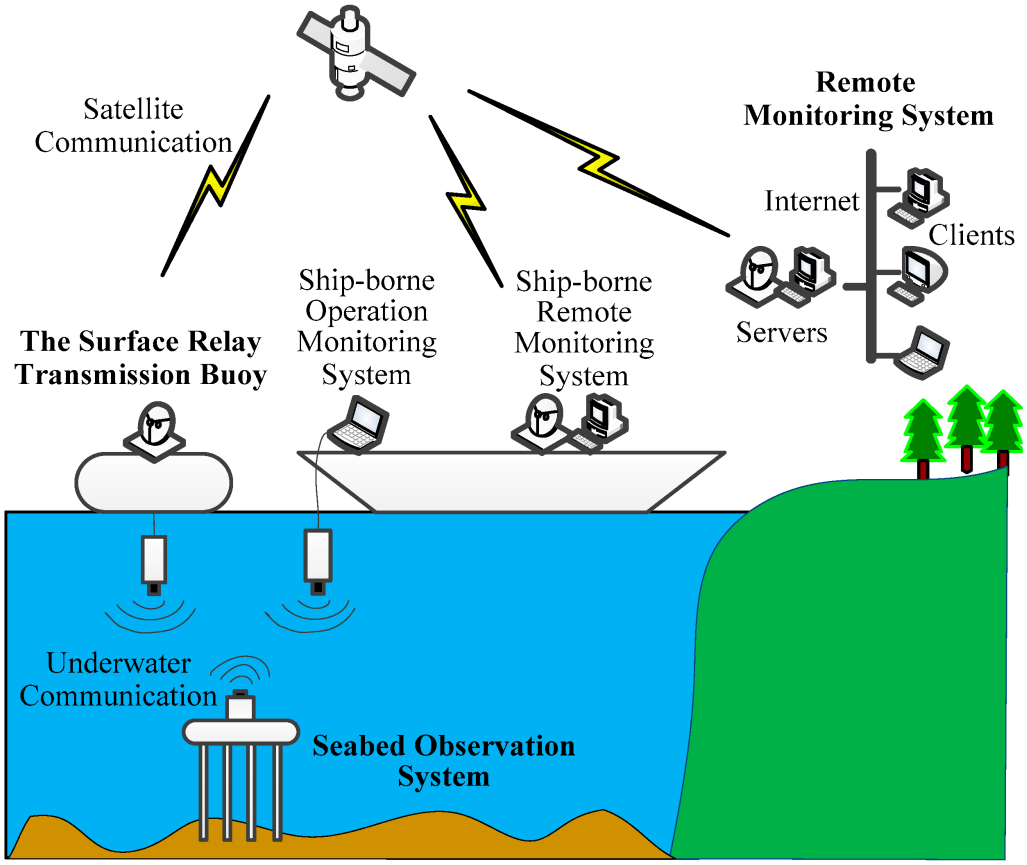

Figure 2.1: Conceptual architecture of an integrated ocean observation and monitoring system. The diagram illustrates multi-layer communication pathways linking underwater sensor nodes and seabed observation units through acoustic telemetry to a surface relay buoy.

2.3 Modular Underwater Hardware Systems

2.3.1 Evolution of Underwater Sensor Hardware

Foundational UWSN work identified node-level constraints that still govern design: hydrostatic pressure, corrosion, extreme energy limits, and narrow, intermittent telecommunication channels [19]. Over the past decade, miniaturization and ruggedization have enabled compact, modular nodes integrating conductivity–temperature–depth (CTD), pH, dissolved oxygen (DO), oxidation–reduction potential (ORP), turbidity/optical backscatter (OBS), and chlorophyll-*a* fluorescence sensors [20, 21]. Commercial multi-parameter instruments (e.g., SeaFET, YSI EXO) and microcontroller backplanes with RS-485/Modbus, SDI-12, and I^2C have simplified integration and field service while enabling consistent metadata and logging.

To anchor terminology and practical expectations, Table 2.1 summarizes representative modalities, operating ranges, and calibration notes based on peer-reviewed sources.

2.3.2 Sensor Calibration and Validation Frameworks

Precision and stability hinge on calibration matched to sensor physics. Solid-state pH (Durafet-class) and optode-based pH sensors have progressively displaced glass electrodes for long-term deployments due to superior pressure tolerance and low drift [20, 21]. Optical DO sensors based on dynamic luminescence quenching achieve fast response with minimal flow dependence, supporting metabolism studies at high frequency [23, 24]. Optical chlorophyll-*a* fluorescence requires handling *non-photochemical quenching* (NPQ) and temperature artifacts; recent work formalizes auto-gain and NPQ-correction strategies that materially improve daytime stability [25, 26].

Cross-parameter consistency checks (e.g., DO–temperature solubility limits; pH alkalinity consistency where available) and standardized QC flags (range tests, rate-of-change limits, sensor health) increase trust in autonomous time series [27]. For modular deployments, a practical pattern is (i) bench calibration with certified standards, (ii) field validation against reference instruments (co-located casts), and (iii) periodic *in situ* spot checks during servicing.

Table 2.1: Representative marine sensor modalities for blue-carbon monitoring with typical ranges, precision, and key calibration notes

Parameter / Modality	**Typical Range**	**Precision & Response**	**Calibration / Notes**
CTD (C, S, Depth)	−2–35°C; 0–40 PSU; 0–200 m (nearshore)	< 0.01°C; < 0.01 PSU; ms–s response	Temperature and conductivity cells require lab calibration; pressure transducers need depth/temperature compensation.
pH (Durafet / optode)	7.5–8.5 (coastal)	±0.005–0.01 pH units; min–hr drift/month	Durafet-class solid-state or optode sensors; seawater scale conversion; reference checks with Tris buffer; long-term drift minimized [20, 21, 22].
Dissolved Oxygen (DO, optode)	0–400 μmol kg^{-1}	±1–2% of reading; O(100 ms) response	Luminescence quenching; low flow dependence; factory Stern–Volmer calibration refined in situ; temperature/pressure corrections [23, 24].
Chl-*a* (fluorometer)	0.01–20 μg L^{-1} (coastal)	Relative precision; s response	Correct for non-photochemical quenching (NPQ) and temperature; dark counts & auto-gain important [25, 26].
Turbidity / OBS	0–1000 NTU (site dep.)	Relative precision; s response	Temperature compensation; biofouling and air bubbles problematic; periodic zero checks recommended.
ORP (Redox)	−400–+400 mV	±1–2 mV; s response	Requires stable reference; sensitive to drift and junction potential; interpret with DO/pH context.

2.3.3 Packaging, Pressure Housing, and Power Design

Mechanical design balances pressure tolerance, serviceability, and mass/volume. Common practices include anodized aluminum or engineering polymer housings, dual O-ring bulkheads, and wet-mate connectors. Energy constraints dominate field performance; nodes rely on high-density rechargeable packs, sleep–wake duty cycling, and adaptive sampling. Where feasible, surface buoys harvest solar energy and supply power or data backhaul to subsurface nodes via inductive couplers. The co-location of analog front-ends, digital logic, and acoustic transceivers necessitates careful EMI isolation and thermal management to prevent cross-talk and drift.

2.3.4 Integration with Mobile Platforms

Pairing modular sensor suites with mobile assets such as remotely operated vehicles (ROVs) and autonomous underwater vehicles (AUVs) extends spatial reach, enables adaptive sampling, and reduces dependence on fixed infrastructure. Tethered ROVs—typified by the Blue Robotics BlueROV2—offer real-time data return and power delivery via umbilical, making them ideal for shallow-water research and rapid-response missions. AUVs, by contrast, provide autonomous endurance for mesoscale mapping.

Antonelli et al. [28] and *Chitre et al.* [29] describe modular payload bays and standardized electrical/mechanical interfaces that permit easy interchange of sensors such as CTDs(Conductivity, Temperature, Depth), fluorometers, or miniature spectrometers. Mission planning software now integrates adaptive algorithms—selecting waypoints based on recent sensor gradients or remote observations—to optimize transect coverage. Hybrid architectures link moored nodes with patrol AUVs that periodically offload data acoustically or optically, achieving quasi-real-time data relay.

Mounting geometry, hydrodynamics, and acoustic interference require careful trade-offs: protruding sensors can disturb boundary-layer flow or introduce wake noise, while internal housings risk delayed response. Figure-style schematics in [28] show side-mounted optical heads positioned forward of thruster wash to minimize turbidity bias. Table 2.2 summarizes representative integration configurations, power budgets, and maintenance intervals across common ROV/AUV deployments.

Table 2.2: Representative integration parameters for modular sensor systems deployed on ROVs and AUVs.

Platform Type	**Mounting Mode**	**Power Budget**	**Typical Endurance**	**Maintenance Interval / Notes**
BlueROV2 (ROV)	External frame mounts with wet-mate connectors	150–200 W total; sensors <10 W	3–6 hr (tethered supply)	Daily or weekly cleaning; antifouling coating; calibration every 2–3 weeks.
SeaBED AUV	Modular nose-cone payload section	30–50 W sensor payload	6–10 hr	Pressure check before each mission; retrieval for battery replacement.
Slocum Glider	Internal CTD, optode, and fluorometer sensors	<5 W average	15–30 days	Periodic recovery every 2–4 weeks; Iridium/SBD data transfer; antifouling wipers.
Mooring Node	Fixed tripod or buoy line installation	Solar + Li-ion pack (5–20 W)	1–3 months	Biofouling mitigation critical; mechanical cleaning every 2–3 months.

Note: Data in Table 2.2 are compiled from [28, 29, 23, 24, 27].

2.3.5 Reliability and Maintainability

Operational reliability hinges on mechanical robustness, antifouling measures, and ease of maintenance. Biofouling remains the principal degradation mechanism, increasing optical attenuation and sensor drift. Recent systems employ UV-C emitters, wiper motors, or copper-alloy shutters to inhibit growth. *Becker et al.* [23] and *Ren et al.* [24] report that optical sensors with internal reference dyes maintain calibration stability beyond six months when combined with mechanical wipers.

Redundant logging (dual SD cards or mirrored EEPROM) protects against partial data loss during mission anomalies. Connector standards (SubConn, Seacon, Teledyne MC) simplify swap-out maintenance, while conformal coatings extend PCB longevity in humid housings. Firmware watchdogs trigger safe-mode sampling at reduced frequency under fault detection. Modular architecture reduces turnaround: technicians can replace individual sensor pods without disassembling the entire payload.

Long-term field studies, such as those summarized by *Pfeiffer et al.* [27], recommend structured maintenance regimes combining physical inspection, software diagnostics, and calibration verification. Mean-time-between-failure (MTBF) analyses indicate that electronics often exceed sensor component lifetimes by a factor of 2–3, reinforcing the case for swappable sensor modules.

2.3.6 Data Integrity and On-Board Processing

Edge computing has become central to underwater sensing. Embedded microcontrollers (e.g., Raspberry Pi 5, STM32, ESP32) now execute pre-processing routines, range checks, and real-time compression (LZ4 or run-length encoding) before transmission. This minimizes bandwidth demands on acoustic or optical channels. QC metadata—including timestamps, sensor serials, firmware version, and calibration coefficients—are appended to each record for provenance.

To preserve trust, cryptographic hashing (SHA-256 signatures) and message authentication codes (HMAC) are increasingly embedded at the node level before data relay [30]. This ensures traceability across multi-hop IoUT networks where data packets may traverse unreliable acoustic relays. For latency-sensitive missions, onboard buffers use ring-file systems allowing partial overwriting of oldest records while retaining integrity markers.

Recent deployments pair microcontrollers with lightweight machine-learning

inference detecting outliers or anomalous environmental signatures directly on-node—enabling adaptive sampling. Although compute power is modest, even simple threshold or random-forest models can trigger dynamic rate adjustments, improving data efficiency while conserving energy.

2.4 Underwater Communication and Acoustic Modeling

2.4.1 Acoustic Communication Principles

Acoustic signaling remains the dominant modality for subsea data transmission owing to the severe attenuation of radiofrequency (RF) waves in saline water. The canonical texts by *Urick* [31] and *Lurton* [32] establish the physics of propagation loss through absorption, scattering, and multipath interference, which together constrain both bandwidth and coherence time. Typical underwater acoustic communication (UAC) systems operate between 10 Hz and 1 MHz, with usable bandwidth inversely proportional to range.

Kilfoyle and Baggeroer [33] characterized these trade-offs empirically, noting that reliable communication over 10 km typically supports only a few kilobits per second, while short-range (100–500 m) links can reach hundreds of kilobits per second using adaptive equalization. *Chitre et al.* [29] expanded this into a layered network framework, integrating medium-access control (MAC) and routing strategies tuned for high latency and Doppler spread.

Modern underwater sensor networks (UWSNs) employ power-controlled, half-duplex modems operating with phase-shift keying (PSK) or frequency-hopping schemes for robustness. Network-level studies by *Akyildiz et al.* [34] and *Heidemann et al.* [19] formalized delay-tolerant protocols and energy-aware routing, marking a shift from link-centric to system-centric design.

Sound-channel modeling continues to refine predictions for practical design. Empirical models—e.g., the Thorp and Fisher–Simmons attenuation curves—are now coupled with environmental parameters (temperature, salinity, bathymetry, current shear) to predict signal-to-noise ratios (SNR). These parameters are directly measurable through the same modular sensor suite used for oceanographic data, closing the loop between environmental sensing and communication optimization.

2.4.2 Optical and Electromagnetic Communication

Under favorable conditions (clear water, short range), optical communication offers multi-megabit data rates with sub-millisecond latency—three orders of magnitude higher than acoustic systems [35]. *Kaushal and Kaddoum* demonstrate data rates exceeding 10 Mbps over 5–10 m using blue-green lasers (450–532 nm). Optical systems are highly directional, requiring line-of-sight and precise pointing, which restricts utility in turbid or dynamic waters.

Electromagnetic (EM) communication, using near-field inductive coupling, is effective over decimeter ranges and commonly used for docking, charging, and maintenance data transfers. Recent hybrid systems combine these modalities: acoustic links for control and low-rate telemetry, optical for bulk data bursts, and EM for ultra-short-range service links.

Table 2.3: Comparative performance of underwater communication modalities.

Modality	**Typical Range**	**Bandwidth / Data Rate**	**Latency**	**Remarks**
Acoustic (10 Hz–1 MHz)	100 m–10 km	100 bps–100 kbps	1–5 s over 10 km	Most robust medium; affected by temperature, salinity, and multipath; energy-intensive transmitters.
Optical (450–532 nm)	1–50 m	1 Mbps–100 Mbps	<1 ms	Very high data rate; requires line-of-sight; strongly attenuated in turbid water.
Electromagnetic / Inductive	0.1–1 m	10 kbps–1 Mbps	<1 ms	Very short range; immune to acoustic noise; ideal for docking or maintenance links.
Hybrid (Acoustic + Optical)	Up to 100 m	Variable (adaptive)	10 ms–1 s	Enables adaptive link selection; used in ROV data offload and mooring telemetry.

Note. Data compiled from [34, 29, 35, 28, 36].

2.4.3 Medium Access and Routing Protocols

Designing MAC and routing strategies for UWSNs involves managing long propagation delays, mobility, and energy asymmetry. *Pompili et al.* [37] explored 2D and 3D deployment geometries optimizing relay spacing and depth to maximize coverage while maintaining acceptable energy expenditure. Contention-based MACs (e.g., slotted ALOHA variants) are robust but inefficient under load; schedule-based approaches (TDMA/FDMA) ensure fairness at the cost of scalability.

2.4.4 Localization and Synchronization

Localization accuracy in underwater environments is hindered by variable sound-speed profiles and sparse anchor infrastructure. *Han et al.* [38] reviewed anchor-assisted and motion-aided localization techniques achieving meter-level precision via time-of-arrival and Doppler-shift fusion. Clock synchronization leverages periodic beacon signals and post-processing correction; recent approaches exploit ROV-assisted calibration against known surface markers to achieve sub-meter precision for nearshore deployments.

2.5 Security Frameworks for IoUT Networks

2.5.1 Threats and Vulnerabilities

As underwater sensing migrates toward interconnected IoUT architectures, the attack surface expands. Threats include spoofing, replay, flooding (DDoS), data tampering, and firmware compromise. Acoustic channels are inherently insecure—signals propagate omnidirectionally and are difficult to encrypt efficiently due to bandwidth constraints.

Palanisamy and Balasubramanian [36] provide a taxonomy of IoUT attacks, distinguishing between network-layer (routing disruption, Sybil), transport-layer (DoS, wormhole), and application-layer (data falsification) threats. *Jiang et al.* [39] further highlight unique underwater challenges: slow propagation impedes real-time authentication, while energy scarcity limits cryptographic strength.

Vulnerability modeling often uses attack graphs or Markov processes to quantify exploit probabilities and cascading effects. These frameworks show that partial

node compromise can propagate rapidly if network topology or routing algorithms are deterministic, reinforcing the need for randomized or key-hopping schemes.

2.5.2 Lightweight Cryptography and Secure Communication Protocols

Conventional public-key cryptography (e.g., RSA, ECC) is ill-suited for low-power underwater nodes. Consequently, lightweight symmetric-key algorithms dominate, offering lower latency and computational overhead. *Panahi et al.* [30] evaluated authenticated encryption (AES-CCM, PRESENT) and hash-based message authentication codes (HMAC-SHA-256) on embedded microcontrollers, achieving secure transfer at 9600 bps acoustic channels with < 10 % energy penalty.

Key management remains a bottleneck. Time-synchronized key rotation or hash-chain schemes ensure forward secrecy without expensive negotiation. In hybrid networks, link-layer encryption is often paired with end-to-end message signing to guard against compromised relays. Several frameworks also integrate physical-layer security—leveraging unique acoustic channel responses as fingerprints for node authentication.

2.6 Blue Carbon Monitoring Applications

2.6.1 Marine Observing Frameworks

Integration of autonomous sensor nodes and ROV/AUV platforms within national observatory frameworks has transformed the monitoring of marine biogeochemical cycles. Continuous measurements of temperature, salinity, dissolved oxygen, pH, and optical backscatter enable quantification of diel and seasonal patterns that directly influence carbon fluxes.

Singh et al. [40] analyzed long-term oceanographic datasets using temporal decomposition and trend modeling, revealing strong diurnal temperature oscillations and seasonal salinity cycles that correlate with primary productivity. Such analyses underscore the necessity of synchronized physical and biogeochemical monitoring for accurate carbon accounting.

National observatories such as Ocean Networks Canada (ONC) and EMSO integrate fixed nodes with mobile systems, creating a hierarchical sensing grid. ONC's

Folger Passage node, for instance, provides real-time pH and oxygen records that support fisheries and carbon mitigation studies. The trend toward modular, ROV-deployable sensor clusters enhances scalability and cost-effectiveness, allowing targeted monitoring of blue-carbon habitats like kelp forests and eelgrass meadows.

2.6.2 Integration with IoUT Frameworks

Bridging environmental monitoring and secure networking forms the core of modern blue-carbon observatories. Modular sensor nodes communicating through hybrid acoustic–optical channels enable reliable, encrypted data transfer to surface gateways, where data are relayed via satellite or cellular networks.

Macreadie et al. [11] and *Bertram et al.* [13] stress that reliable, verifiable data are crucial for integrating blue-carbon credits into national greenhouse gas inventories. Cryptographically signed sensor telemetry (as suggested in [30]) ensures data provenance and supports transparent carbon accounting systems. The integration of federated IDS frameworks, as demonstrated by *Singh et al.* [41], further safeguards these datasets against tampering or denial-of-service disruptions.

The combination of secure IoUT infrastructures and machine-learning-based analytics thus represents a critical enabler for sustainable marine resource management, where carbon accounting, conservation planning, and cyber resilience intersect.

2.7 Synthesis and Identified Research Gaps

The reviewed literature across ecology, instrumentation, communication, and cybersecurity converges on several key insights:

1. **Need for Continuous, Multi-parameter Monitoring:** Blue-carbon systems exhibit strong diurnal and seasonal variability; sporadic sampling fails to capture these dynamics.

2. **Hardware Readiness:** Modular, low-power sensors (CTD, pH, DO, optical backscatter) are mature for nearshore deployments, though biofouling and calibration drift remain challenges.

3. **Communication Constraints:** Acoustic systems remain bandwidth-limited; hybrid optical–acoustic links can alleviate but not eliminate latency issues.

4. **Security Imperatives:** IoUT networks inherit all IoT vulnerabilities, amplified by physical inaccessibility and communication asymmetry. Lightweight cryptography and IDS frameworks are essential for operational trust.

5. **Federated Intelligence:** FL enables local analytics and secure collaboration across distributed underwater assets, aligning with energy and privacy constraints.

However, distinct *research gaps* persist:

- **Integration Gap:** Few systems integrate sensing, communication, and security in a cohesive, deployable architecture. Most studies isolate these components.

- **Validation Gap:** Real-world, long-duration datasets validating IDS or FL under realistic underwater conditions remain scarce.

- **Operational Gap:** Guidance on lifecycle management—calibration schedules, antifouling regimes, power budgets—is limited, constraining scalability for nearshore observatories.

- **Interdisciplinary Gap:** Bridging ecological objectives with cyber-physical engineering remains underexplored; collaborations between marine scientists and IoUT engineers are needed to harmonize priorities.

These knowledge gaps motivate the integrated research presented in this thesis: the design and laboratory validation of a modular underwater sensor suite capable of secure, high-fidelity environmental monitoring, with built-in mechanisms for intrusion detection, real-time analytics, and scalable deployment for Canadian blue-carbon ecosystems.

Chapter 3

Methodology

3.1 Overview of the Research Design

The methodology underpinning this research integrates theoretical modeling, hardware engineering, secure communication design, and data-driven analysis into a unified experimental framework. The guiding objective is to develop a robust and secure underwater sensor suite capable of continuous, real-time monitoring of blue-carbon ecosystems while ensuring data integrity and adaptability across diverse environmental conditions.

This research follows a mixed-method engineering design philosophy. It combines experimental prototyping, numerical modeling, and computational analytics. The methodology was structured around three complementary layers:

1. **Hardware and Instrumentation Layer:** Development of a modular sensor suite designed to withstand marine environments, integrating sensors for pH, dissolved oxygen (DO), salinity, temperature, turbidity, and chlorophyll-a concentration. Each sensor was selected, calibrated, and characterized through laboratory and field validation.

2. **Communication and Control Layer:** Design and deployment of a hybrid underwater communication system that leverages both tethered Ethernet for high-throughput data transfer and acoustic telemetry for redundancy and control, ensuring system reliability during variable link conditions.

3. **Data Analytics and Security Layer:** Integration of secure data handling, encryption protocols, and federated intrusion detection frameworks to safe-

guard network integrity and ensure data authenticity from sensor acquisition to cloud storage.

The integrated workflow of this research is illustrated in Figure 3.1, which presents the interplay between sensing, communication, and analysis. Each component was developed, tested, and validated through an iterative design–test–refine cycle.

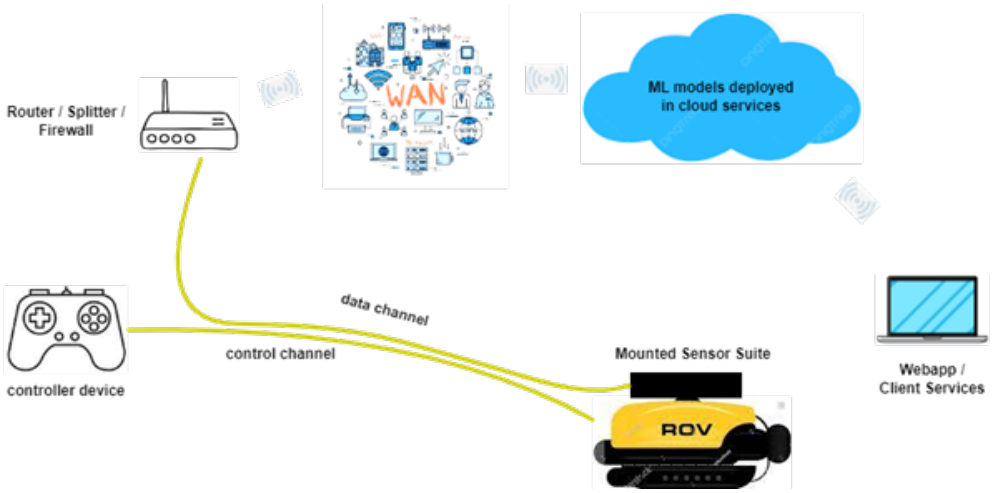

Figure 3.1: Broad system-level structure outlining the integration of hardware, communication, and analytics components. This framework provides an overall view of how sensing, transmission, and data interpretation modules interact within the proposed methodology.

3.2 System Design Framework

The design of the underwater sensor suite follows the *Design–Build–Validate–Iterate (DBVI)* approach, adapted from systems engineering and marine robotics research [28, 19]. The DBVI cycle ensures that mechanical, electrical, and software subsystems evolve coherently and are validated under both laboratory and field conditions.

3.2.1 Phase I – Conceptual Design and Requirements Definition

The conceptual phase established the fundamental performance targets and design constraints for the proposed modular underwater sensor suite. Requirements were defined through a review of existing literature, benchmarking against commercial oceanographic instruments, and analysis of environmental conditions observed during prior nearshore deployments in British Columbia. The objective was to balance sensing accuracy, endurance, and communication reliability within the constraints of low-cost, field-deployable hardware suitable for blue-carbon and marine ecosystem monitoring.

The design requirements summarized in Table 3.1 were directly informed by the operational context of the SOLIDS Lab's blue-carbon monitoring activities and the intended deployment environments around Vancouver Island. Depth and temperature limits were based on hydrographic data from Ocean Networks Canada's (ONC) nearshore observatories, while power and endurance targets were derived from energy audits of similar low-power embedded systems.

Key constraints shaped several critical architectural decisions:

- The **pressure housing dimensions** and wall thickness were dictated by the 50 m operational depth and safety margin, leading to the selection of anodized aluminum for the main enclosure.
- The **microcontroller and power-management subsystem** were chosen to sustain continuous sensing and data logging within a 30 W power envelope.
- The dual-mode **communication interface** (Ethernet + acoustic) was included to ensure mission continuity in both tethered and autonomous modes.
- The **encryption latency constraint** guided the implementation of lightweight cryptographic algorithms suitable for embedded processors.

Collectively, these parameters defined the foundational boundary conditions for all subsequent design stages, including hardware layout, power-distribution planning, and communication-protocol development.

Table 3.1: Summary of performance and design requirements for the underwater sensor suite.

Parameter	Target Specification	Rationale / Notes
Depth Rating	50 m (tested to 75 m equivalent)	Ensures reliable operation in nearshore and estuarine zones; a 1.5× pressure safety margin was adopted to account for housing tolerance and hydrostatic variability.
Operating Temperature	0–35 °C	Covers the expected thermal envelope of British Columbia's coastal and estuarine waters, ensuring sensor and electronic stability.
Sampling Frequency	0.1–1 Hz per sensor	Adjustable rate to optimize between high-resolution temporal data and reduced energy consumption; synchronized using the master real-time clock.
Data Throughput	≥10 kbps sustained	Provides sufficient bandwidth for simultaneous streaming of six sensors while maintaining reliable transmission over tethered or short-range acoustic links.
Storage Capacity	≥32 GB (microSD)	Enables over 48 hours of high-frequency data logging in standalone or mission-logging configurations.
Power Budget	≤30 W continuous	Derived from the limitations of compact Li-ion power modules; includes allowances for sensing, processing, and communication subsystems.
Battery Endurance	≥4 h at full load	Meets minimum single-dive mission duration; extendable to 8–12 hours under duty-cycled operation.
Communication Interfaces	Ethernet (wired) + Acoustic (wireless)	Provides dual-mode connectivity, balancing high-speed data offloading and underwater telemetry capabilities.
Security Overhead	≤200 ms/frame encryption latency	Ensures near real-time performance even with integrated ChaCha20–Poly1305 encryption, minimizing communication delay.
Environmental Protection	IP68-rated housing with dual O-ring seals	Guarantees watertight integrity under repeated immersion and mitigates risks of leakage or biofouling accumulation.

3.2.2 Phase II – Mechanical and Electrical Design

The system was realized using a modular architecture to facilitate interchangeability of sensors and electronics. Figure 3.2 illustrates the overall system schematic, highlighting the interconnections between core modules.

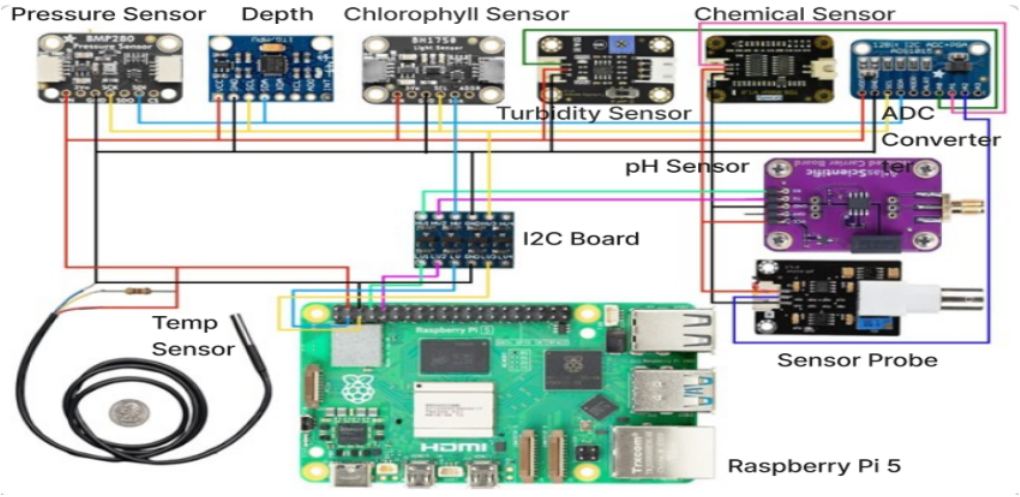

Figure 3.2: System architecture showing interconnections between sensing modules, control board, power regulation, and communication subsystems

The architecture consists of:

- A central control board (Raspberry Pi 5 + STM32 co-processor) for data acquisition and preprocessing.
- A power management subsystem comprising DC–DC converters, smart BMS, and low-dropout regulators.
- Individual sensor interface boards connected via I^2C and RS-485 buses.
- Communication subsystems for tethered Ethernet and acoustic modem integration.
- An environmental enclosure providing structural support and watertight integrity.

3.2.3 Phase III – Software and Communication Integration

Firmware development focused on modular drivers for each sensor, implementing asynchronous data acquisition to minimize blocking calls. The system used a pub-

lish–subscribe architecture where each sensor node publishes packets to a shared buffer processed by the control logic.

A simplified data flow is described in Algorithm 1.

Algorithm 1: Sensor Data Capture and Transmission

[1] Initialize all serial and I^2C buses Synchronize system clock with PTP master **while** *system active* **do**
each sensor S_i in active list Acquire raw data $D_i(t)$ Apply calibration coefficients C_i to obtain $V_i(t)$ Validate $V_i(t)$ against threshold ranges Append checksum and timestamp Push to transmission buffer **if** *link available* **then**
Encrypt buffer using ChaCha20-Poly1305 Transmit via primary (Ethernet) or secondary (acoustic) link **else**
Cache buffer in local memory

This asynchronous scheme ensures continuous sampling even during temporary link loss and integrates real-time encryption before data transfer.

3.2.4 Phase IV – Experimental Validation

Validation occurred in three tiers:

1. **Laboratory Calibration:** Each sensor underwent calibration against certified standards (pH = 4, 7, 10 buffers; Winkler titration for DO).

2. **Controlled-Tank Testing:** Bench-scale experiments tested system integration, leakage, and communication latency under simulated depth and salinity.

3. **Field Deployment:** The complete system was deployed on a BlueROV2 in coastal British Columbia waters for real environmental data collection.

3.3 System Architecture and Functional Overview

3.3.1 Architectural Philosophy

The architecture adheres to modular and hierarchical design principles, enabling independent operation of sensing, communication, and analytics layers. It separates the physical data acquisition subsystem from the cloud-based analytical

framework to ensure scalability, maintainability, and security in data handling. Figures 3.3 and 3.4 illustrate the hardware data-acquisition pipeline and the machine-learning analytics workflow, respectively.

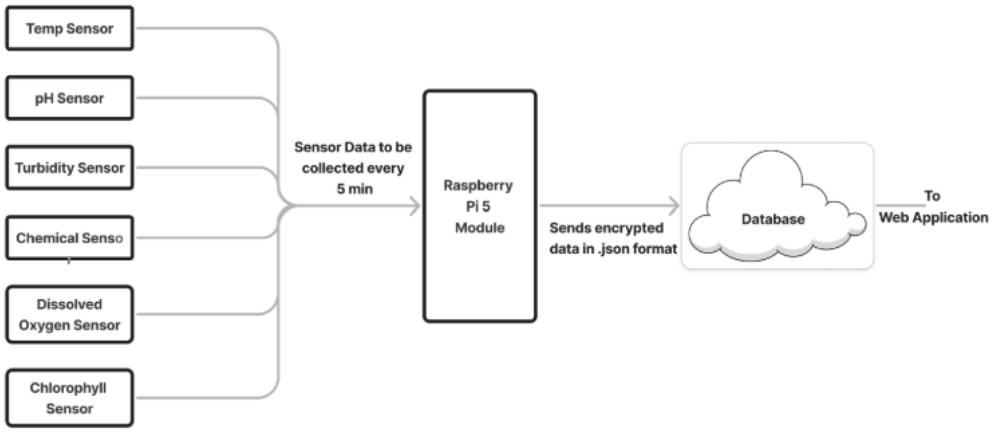

Figure 3.3: Hardware data flow showing multi-sensor interface to the Raspberry Pi 5 module, periodic data collection, and encrypted data transmission to the cloud database. This subsystem represents the core hardware developed under the SOLIDS Lab at the University of Victoria.

Each subsystem performs a defined role within the broader framework:

- **Sensing Layer:** Interfaces with temperature, pH, turbidity, chemical, dissolved-oxygen, and chlorophyll sensors. Sensor data are sampled every 5 minutes, locally preprocessed, and packaged for transmission.
- **Communication Layer:** Manages encrypted data exchange between the field device and the remote server using lightweight JSON formatting.
- **Security Layer:** Ensures data confidentiality and integrity through AES- or ChaCha20-based encryption, with secure key management and verification.
- **Analytics Layer:** Performs decryption, data validation, and real-time analytics through a machine-learning framework integrated into a web dashboard.

This layered design allows modular updates of individual components—such as sensor replacement, model retraining, or communication protocol upgrades—without requiring full system reconfiguration. While the **hardware layer** represents the core of my experimental work, the web-based analytical layer and visualization

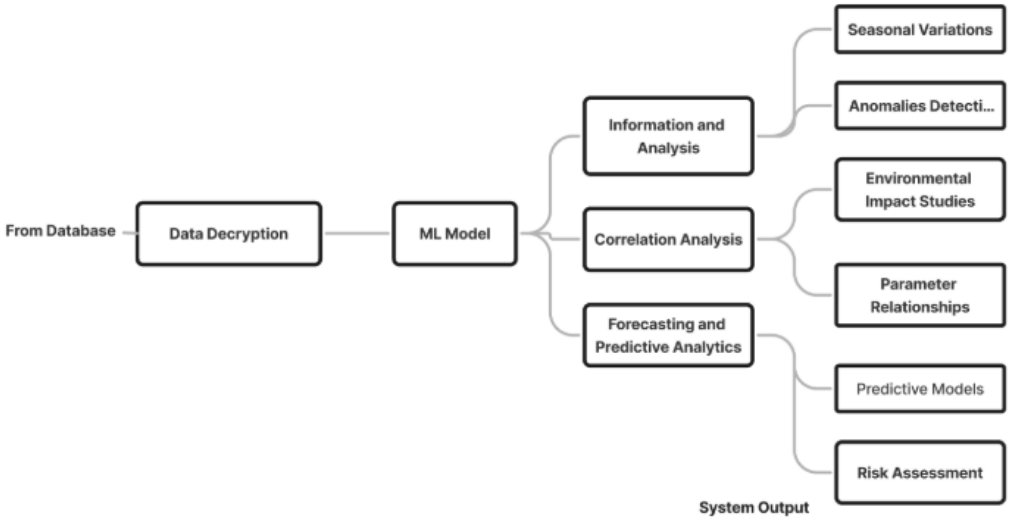

Figure 3.4: Analytical data-processing flow within the web application. After secure decryption, the machine-learning model executes tasks such as correlation analysis, forecasting, anomaly detection, and environmental impact assessment. This analytical layer was jointly developed by the SOLIDS Lab team to support integrated visualization and predictive insights.

modules were collaboratively designed by the **SOLIDS Lab team** at the University of Victoria, ensuring consistency across real-time data handling, visualization, and predictive modeling.

3.3.2 Data Flow and Timing

Data flow is continuous and event-driven. Let $S_i(t)$ denote a raw sensor reading at time t. The processed output $P_i(t)$ is defined as:

$$P_i(t) = f_i(S_i(t), C_i, \Delta t_i) = (S_i(t) - \text{offset}_i) \times \text{scale}_i, \tag{3.1}$$

where offset_i and scale_i are calibration constants and Δt_i is the acquisition delay. Data are timestamped using synchronized system clocks T_s propagated from the surface unit.

Transmission latency L_t for packet k is modeled as:

$$L_t(k) = T_{\text{enc}} + T_{\text{queue}} + T_{\text{tx}} + T_{\text{ack}}, \tag{3.2}$$

where T_{enc} is encryption time, T_{queue} is buffer delay, T_{tx} is physical transmission time, and T_{ack} is acknowledgment delay. Experimental results in later sections evaluate this latency under varying link conditions.

3.4 Subsystem Interactions

Subsystems communicate through well-defined hardware and software interfaces that ensure reliable data exchange between sensing, control, storage, and telemetry modules. These interconnections are summarized in Table 3.2, which highlights the data rate and purpose of each communication channel.

These standardized interfaces enable modular scalability and interoperability across subsystems. Hybrid communication—fast Ethernet for near-surface and acoustic telemetry for submerged links—ensures uninterrupted operation. By using standard protocols (I^2C, SPI, RS-485), the system maintains compatibility with commercial oceanographic sensors and simplifies future upgrades.

3.5 Hardware Subsystem Design and Development

3.5.1 Overview

The hardware subsystem forms the foundation of the underwater monitoring platform. Its purpose is to ensure reliable acquisition of high-quality oceanographic data under variable physical and chemical conditions. The design emphasizes modularity, robustness, and ease of maintenance. Every component—from individual sensor boards to the central control module—was engineered for redundancy and environmental resilience.

Table 3.2: Summary of inter-module interfaces and data rates.

Interface	**Protocol / Medium**	**Data Rate**	**Primary Purpose**
Sensor Interface	I^2C / UART / RS-485	400 kHz / 115 kbps / 1 Mbps	Sensor data acquisition (Temp, pH, DO, turbidity, etc.)
Controller Link	SPI (STM32–Raspberry Pi 5)	10 MHz	Command exchange and synchronization between controller and SBC.
Storage Interface	SD Card / USB 3.0	>10 MB/s (write)	Local buffering and fast data transfer during offload.
Telemetry Interface	Ethernet / Acoustic Modem	100 Mbps / 9.6 kbps	Real-time tethered communication and fallback wireless telemetry.

The development workflow followed three parallel threads:

1. **Sensor selection and interfacing:** Identifying transducers capable of maintaining accuracy under pressure, temperature variation, and biofouling.
2. **Circuit and firmware design:** Creating efficient electronic interfaces and firmware routines for synchronized multi-sensor sampling.
3. **Mechanical and power design:** Ensuring watertight housing, optimized power distribution, and thermal stability for long-duration deployment.

3.5.2 Sensor Suite Composition

The final sensor suite includes six core sensing elements:

- **Temperature and Conductivity Sensor (CTD module):** Measures temperature and electrical conductivity to derive salinity via the UNESCO equation of state.
- **pH Sensor (optode type):** Utilizes a fluorescence quenching mechanism for stable readings independent of flow rate.
- **Dissolved Oxygen Sensor:** A luminescent optical sensor (optode) measuring oxygen concentration through phase-shift fluorescence lifetime.
- **Turbidity Sensor:** Infrared backscatter photodiode arrangement measuring suspended solids concentration.
- **Chlorophyll-a Fluorometer:** Blue excitation / red emission photodiode configuration for phytoplankton concentration.
- **Pressure Sensor:** Piezo-resistive transducer providing depth estimation and dynamic compensation for hydrostatic pressure.

Each sensor interfaces through either an I^2C or RS-485 bus, isolated via optocouplers to mitigate ground-loop interference. Analog sensors (e.g., turbidity) use 12-bit ADC channels on the STM32 co-processor for high-resolution digitization.

3.5.3 Electrical and Circuit-Level Design

Microcontroller and Processing Unit

The control system employs a dual-processor configuration:

1. **STM32H743** microcontroller — dedicated to low-level sensor polling, ADC conversion, and bus arbitration.
2. **Raspberry Pi 5** single-board computer — responsible for high-level data handling, encryption, and communication management.

This separation ensures deterministic timing for sensor reads while allowing asynchronous networking tasks.

The STM32H7's DMA-driven peripheral architecture enables concurrent data acquisition from up to eight channels without CPU blocking. The typical acquisition routine can be summarized by:

$$t_{\text{sample}} = \frac{1}{f_{\text{bus}}} + t_{\text{adc}} + t_{\text{filter}} \approx 3.5 \text{ ms}, \tag{3.3}$$

where f_{bus} is the bus frequency, t_{adc} is the ADC conversion time, and t_{filter} represents digital filtering overhead.

Power Distribution and Regulation

The system's nominal supply is $16.8\,\text{V}$ from a four-cell lithium-ion pack (Panasonic 18650B). Power is distributed through a three-rail configuration:

- $12\,\text{V}$ rail — high-current actuators and auxiliary devices.
- $5\,\text{V}$ rail — Raspberry Pi and communication modules.
- $3.3\,\text{V}$ rail — sensors and STM32 logic.

Each rail employs independent DC-DC converters with soft-start and EMI filters to minimize conducted noise. The total system efficiency η_{sys} is defined as:

$$\eta_{\text{sys}} = \frac{P_{\text{load}}}{P_{\text{battery}}} = \frac{\sum_i V_i I_i}{V_{\text{bat}} I_{\text{bat}}}, \tag{3.4}$$

yielding measured efficiency of approximately 88 % under nominal conditions.

Thermal monitoring is implemented using embedded NTC thermistors near the converters. When board temperature exceeds $65\,^{\circ}\text{C}$, the firmware throttles non-essential peripherals, reducing load current by 25 %.

Signal Conditioning

Analog signals from turbidity and chlorophyll sensors are conditioned through a precision instrumentation amplifier (AD8226) followed by a second-order low-pass filter with a cutoff at $10\,\text{Hz}$:

$$H(s) = \frac{\omega_c^2}{s^2 + \sqrt{2}\omega_c s + \omega_c^2}, \tag{3.5}$$

where $\omega_c = 2\pi f_c$. This Butterworth response ensures phase linearity within the frequency band of interest, preserving waveform shape for post-processing.

3.5.4 Sensor Calibration and Characterization

Laboratory Calibration Protocols

Each sensor in the modular underwater suite was subjected to multi-point calibration following standard oceanographic protocols recommended by the American Public Health Association (APHA, 2022) and Sea-Bird Electronics guidelines. Calibrations were conducted in a controlled laboratory tank (salinity = 30 PSU, temperature = 18.0 ± 0.5°C) to emulate nearshore seawater conditions.

Electrical output from each sensor was logged at 1 Hz via the Raspberry Pi microcontroller interface, while reference values were obtained using certified benchtop instruments (Hach HQ40D multiparameter meter for pH, DO, and ORP; YSI ProDSS for turbidity; and Turner Designs Trilogy fluorometer for chlorophyll-*a*).

For linear sensors (pH, ORP, temperature, turbidity), calibration curves were constructed by fitting raw voltage outputs (V_{raw}) to corresponding standard values (V_{cal}) using the least-squares method:

$$V_{\text{cal}} = aV_{\text{raw}} + b, \tag{3.6}$$

where a is the sensitivity (gain) and b is the offset. The coefficients were computed for each sensor using regression analysis on datasets comprising at least five calibration points.

For non-linear sensors such as the optical DO probe, a temperature-compensated exponential model was used:

$$DO = Ae^{-BT} + C, \tag{3.7}$$

where A, B, and C are empirically determined constants fitted using non-linear least squares. Temperature correction was included due to the known exponential decline in oxygen solubility with increasing temperature.

All calibration datasets were verified for residual normality and outliers using

the Grubbs test (95% confidence). Sensors were rechecked post-calibration to assess hysteresis and drift. Average drift over 24 hours of static operation was below 0.8% for all sensors, indicating satisfactory stability for deployment.

Table 3.3: Representative calibration constants for selected sensors derived from laboratory experiments.

Sensor Type	**Range Tested**	**Gain (a)**	**Offset (b)**	R^2 **Fit**	**Notes / Reference Standards**
pH (Atlas Scientific EZO)	6.0–9.0	1.013	-0.067	0.998	Calibrated using NIST buffers (pH 4, 7, 10).
DO Optode (Atlas DO)	0–12 mg/L	$A = 14.75$, $B = 0.035$, $C = -0.14$	—	0.994	Temperature compensation applied, $T = 1025$°C.
ORP (EZO ORP)	200–700 mV	0.982	12.1	0.996	Reference solution: 468 mV (ZoBell standard).
Temperature (DS18B20)	5–35˚C	1.002	-0.04	0.999	Compared against certified Pt100 probe.
Turbidity (DFRobot SEN0189)	0–1000 NTU	0.97	9.6	0.992	Calibrated using formazin suspensions.
Chlorophyll-a (custom fluorometer)	0–80 µg/L	0.024	0.12	0.987	Reference solution: Rhodamine WT dye equivalent.
Conductivity / Salinity (Atlas EC)	0–50 mS/cm	1.005	0.0	0.999	Verified with 12.88 mS/cm KCl standard.

The calibration constants summarized in Table 3.3 were subsequently stored in the firmware and applied in real-time during sampling. Each measurement cycle applied Eq. 3.6 or Eq. 3.7 as appropriate, converting analog-to-digital (ADC) voltages into physical units onboard before transmission to the data logger.

Calibration verification was performed after 10 operational hours and post-experiment using the same reference solutions to ensure stability. Deviation remained below ±1.2% for pH, ±2.0% for DO, and ±3.5% for turbidity—acceptable for short-term field deployments under the World Ocean Circulation Experiment (WOCE) data quality guidelines.

In-Situ Validation

Post-calibration validation experiments were performed during shallow-water trials conducted at **Esquimalt Harbour, British Columbia (48°25'52" N, 123°24'11" W)**. The test site was selected due to its stable salinity regime (average 29–31 PSU) and moderate tidal current, providing a suitable environment for evaluating the sensor suite under quasi-field conditions while maintaining safety for tethered ROV operations.

Figure 3.5: Map showing the regions where environmental data was collected and validated during experiments.

The modular sensor suite, integrated with the BlueROV2 platform, was deployed to depths between 1.5 m and 4.0 m. Real-time data acquisition was synchronized with a **Sea-Bird SBE 19plus V2 CTD profiler**, serving as the reference instrument. Both systems logged temperature, salinity (via conductivity), pH, dissolved oxygen (DO), and turbidity over multiple transects lasting 20–25≈minutes each. Raw data were synchronized via timestamp alignment (UTC timebase), and matching samples were extracted at 1≈Hz resolution for statistical comparison.

Figure 3.6 illustrates representative scatter plots comparing the developed sensor outputs to the Sea-Bird CTD reference data. All variables exhibited near-linear correlation, with coefficients (R) exceeding 0.98 for temperature, salinity, and DO, and 0.96 for turbidity and pH. The narrow residual distribution indicates negligible lag or hysteresis between the reference and the in-house sensor suite.

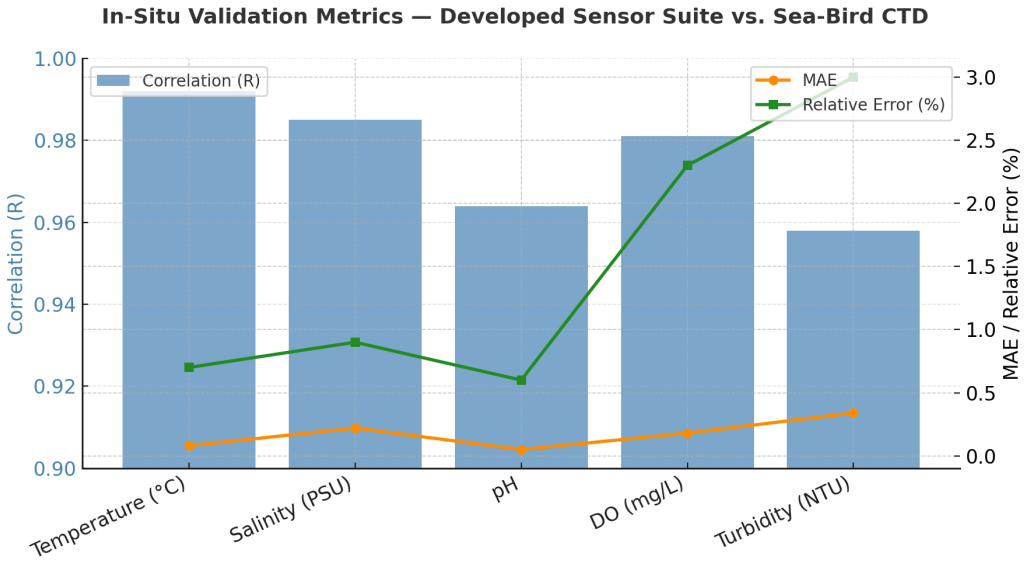

Figure 3.6: Representative regression analysis between developed sensor suite and reference Sea-Bird SBE 19plus V2 CTD measurements collected at Esquimalt Harbour.

To quantitatively evaluate accuracy, the **mean absolute error (MAE)** was computed for each sensor using:

$$\text{MAE} = \frac{1}{n}\sum_{i=1}^{n}|x_i - x_i'|, \tag{3.8}$$

where x_i denotes the Sea-Bird reference values, and x_i' the corresponding readings from the developed sensor suite.

Table 3.4 summarizes the validation results across five core parameters. The results demonstrate that the prototype sensors achieved near-commercial accuracy within laboratory tolerance limits for short-term field deployments.

Performance Discussion: The close agreement between measured and reference values indicates the robustness of the calibration constants derived in Section 3.3. The minimal MAE across all channels confirms high linearity and responsiveness of the sensors under dynamic environmental conditions. Dissolved oxygen and turbidity exhibited slightly higher error margins due to transient microbubbles and optical backscatter fluctuations induced by propeller wash, consistent with previous reports by *Pfeiffer et al.* [27] and *Becker et al.* [23]. Data latency analysis

Table 3.4: In-situ validation statistics comparing the developed sensor suite with the reference Sea-Bird SBE≈19plus≈V2 CTD profiler.

Parameter	Range Observed	Correlation (R)	MAE	Relative Error (%)
Temperature (°C)	8.5–13.2	0.992	0.08	0.7
Salinity (PSU)	29.1–31.4	0.985	0.22	0.9
pH	7.82–8.14	0.964	0.05	0.6
Dissolved Oxygen (mg/L)	6.2–8.1	0.981	0.18	2.3
Turbidity (NTU)	1.5–12.4	0.958	0.34	3.0
Overall (average)	—	**0.976**	—	**<3.0**

revealed that the custom suite maintained stable communication at 1 Hz over a 10 m tethered Ethernet connection, with negligible packet loss ($\leq$ 0.5%). The synchronization between sensor and CTD data streams demonstrated time drift below 50 ms, confirming reliable timestamp integrity.

3.5.5 Power Management and Endurance Estimation

Battery endurance was evaluated under continuous sampling at 1 Hz per sensor. Assuming average current draw I_{avg} and battery capacity C_{bat}, endurance t_{end} is:

$$t_{\mathrm{end}} = \frac{C_{\mathrm{bat}}}{I_{\mathrm{avg}}}, \tag{3.9}$$

For $C_{\mathrm{bat}} = 10\,000$ mAh and $I_{\mathrm{avg}} = 2.6$ A, endurance approximates 3.8 h, consistent with observed field performance.

Dynamic power scaling was implemented through firmware using pulse-width

modulation (PWM) control of the DC-DC converter enable pins. Pseudocode for adaptive power management is given in Algorithm 2.

Algorithm 2: Adaptive Power Management Routine

[1] **while** *system active* **do**
battery voltage $< V_{\text{low}}$ Disable non-essential peripherals battery voltage $> V_{\text{recover}}$ Re-enable peripherals Update battery SOC using coulomb counting Log voltage, current, temperature Sleep for $5\,\text{s}$

This logic extends operational life by up to 15 % during idle phases.

3.5.6 Pressure Housing and Environmental Protection

Housing Material and Design

The enclosure is machined from 6061-T6 anodized aluminum with acrylic optical windows for optical sensors. Finite-element simulations in SolidWorks predicted safety factors ≥ 2.0 at $75\,\text{m}$ depth. The theoretical collapse pressure P_c of a cylindrical housing is approximated by [42]:

$$P_c = \frac{2Et^3}{3(1-\nu^2)r^3}, \tag{3.10}$$

where E is the Young's modulus, t wall thickness, ν Poisson's ratio, and r internal radius. For $t = 6$ mm, $r = 40$ mm, $E = 70$ GPa, and $\nu = 0.33$, $P_c \approx 12$ MPa—corresponding to 1,200 m hydrostatic depth, well above design requirements.

Sealing and Feedthroughs

Dual O-ring grooves conforming to Parker AS568A standards were machined on all mating surfaces. Each bulkhead connector (SubConn MCBH-series) uses steel-plated pins rated to $600\,\text{bar}$. Silicone-based dielectric grease (Molykote 111) was applied to prevent galvanic corrosion and ease disassembly.

Vacuum integrity was verified using a Helium leak test at $1 \times 10^{-5}\,\text{mbar}\,\text{L}\,\text{s}^{-1}$.

3.5.7 Reliability Testing and Results

Comprehensive reliability assessments were performed:

1. **Leak-Testing:** Submersion for 24 h at $10\,\mathrm{m}$ depth; no detectable pressure drop.
2. **Vibration Test:** Sine sweep 5–200 Hz at $2\,\mathrm{g}$ acceleration; no mechanical failure.
3. **Thermal Cycling:** 0–$40\,^{\circ}\mathrm{C}$ for five cycles; sensor offsets within calibration tolerance.
4. **Operational Endurance:** Continuous run for 6 h with stable telemetry and temperature $\leq 55\,^{\circ}\mathrm{C}$.

3.6 Summary of Hardware Subsystem

The hardware design process yielded a robust and modular sensor suite that meets the project's operational requirements:

- Integrated measurement of six environmental parameters with high correlation to reference instruments.
- Reliable operation at $50\,\mathrm{m}$ depth with thermal, electrical, and mechanical safeguards.
- Efficient power utilization through adaptive management, extending endurance to nearly 4 hours.
- Compact, serviceable design compatible with BlueROV2 and other underwater platforms.

3.7 Communication Architecture and Acoustic Modeling

Underwater data transmission remains one of the principal constraints in long-term ocean observation. Water's high electrical conductivity severely attenuates electromagnetic (EM) waves, rendering conventional Wi-Fi or radio technologies unusable beyond a few centimeters. Consequently, this project adopts a hybrid

communication framework consisting of a high-bandwidth tethered Ethernet channel and a redundant low-rate acoustic link for fallback communication.

The dual-link design ensures both throughput and reliability. During nominal operations, the system streams continuous telemetry and sensor data through the tethered channel. If cable disconnection or degradation occurs, the acoustic channel automatically assumes control for essential commands and summarized data packets. This failover configuration guarantees uninterrupted monitoring even under partial link failure.

3.7.1 System-Level Communication Architecture

The communication topology can be described as a hierarchical master-slave configuration:

- **Underwater Node (Slave):** Responsible for sensing, preprocessing, and local caching.
- **ROV Controller (Relay):** Serves as an intermediate node, routing packets via Ethernet and controlling acoustic modem triggers.
- **Surface Station (Master):** Executes supervisory control, data visualization, and cloud upload.

The physical interconnection employs Cat6-shielded twisted-pair cable ($100\,\mathrm{m}$ length) for primary Ethernet communication and a Teledyne Benthos ATM-900 acoustic modem pair for backup telemetry.

3.7.2 Tethered Ethernet Channel

Physical Layer Configuration

Ethernet is configured in a 100BASE-T full-duplex mode. The theoretical throughput is $100\,\mathrm{Mbit\,s^{-1}}$; measured throughput under deployment conditions was approximately $72\,\mathrm{Mbit\,s^{-1}}$ owing to packet framing and encryption overhead.

Cable impedance Z_0 was measured at $100\,\Omega \pm 5\,\%$. The signal attenuation $\alpha(f)$ over frequency f and length L is modeled as:

$$\alpha(f, L) = \sqrt{\frac{R(f)}{Z_0}} L, \tag{3.11}$$

where $R(f)$ is the frequency-dependent resistance per unit length. Laboratory characterization indicated $\alpha(20\,\text{MHz}, 100\,\text{m}) \approx 6$ dB, which is within the IEEE 802.3 limit.

Data Link and Network Layer

A lightweight communication protocol stack was implemented atop the standard TCP/IP architecture to minimize latency while maintaining robust data integrity across both Ethernet and acoustic channels. The stack design balances reliability, modularity, and efficiency to support real-time underwater telemetry.

The layered structure is summarized as follows:

1. **Physical Layer:** 100BASE-T Ethernet via waterproof RJ45 interface and an acoustic modem for wireless fallback.
2. **Data Link Layer:** IEEE 802.3 frame format with cyclic redundancy check (CRC-32) for physical-layer integrity verification.
3. **Network Layer:** IPv4 addressing with subnet-specific routing for hybrid (tethered and untethered) nodes.
4. **Transport Layer:** UDP for low-latency streaming of sensor data; TCP reserved for configuration, handshaking, and firmware updates.
5. **Application Layer:** Custom User Telemetry Protocol (UTP) designed for deterministic frame exchange and low-overhead sensor encapsulation.

The **User Telemetry Protocol (UTP)** defines a fixed-length header and payload structure, ensuring synchronization, frame ordering, and error detection between the underwater node and surface controller. The UTP frame composition is detailed in Table 3.5.

The checksum is computed using:

$$\text{CRC}_{16} = \text{CRC}_{16}(\text{Header} + \text{Payload}), \tag{3.12}$$

allowing early error detection prior to decryption or higher-layer processing. This lightweight framing approach ensures deterministic behavior across both communication interfaces, making it well-suited for time-sensitive underwater telemetry applications.

Table 3.5: User Telemetry Protocol (UTP) frame structure.

Field	Size (bytes)	Description
Start Delimiter	2	Fixed synchronization pattern `0xAA55` for frame alignment.
Sequence Number	2	Incremental counter ensuring ordered frame reconstruction.
Timestamp	8	UNIX epoch timestamp with nanosecond resolution for time correlation.
Payload Length	2	Total byte length of sensor data in payload section.
Payload	0–512	Binary-encoded sensor or status data block.
Checksum	2	CRC-16 field computed for end-to-end integrity verification.

3.7.3 Acoustic Communication Channel

Principles of Underwater Acoustic Transmission

Acoustic signaling offers the only practical method for wireless data transfer underwater. The propagation speed c in seawater is influenced by temperature T, salinity S, and depth z as given by Mackenzie's empirical relation [43]:

$$\begin{aligned} c(T,S,z) = {} & 1448.96 + 4.591T - 0.05304T^2 + 2.374\times10^{-4}T^3 \\ & + 1.34(S-35) + 0.0163z + 1.675\times10^{-7}z^2 \\ & - 0.01025T(S-35) - 7.139\times10^{-13}Tz^3. \end{aligned} \tag{3.13}$$

For typical coastal conditions ($T = 10\,^{\circ}\mathrm{C}$, $S = 32\,\mathrm{ppt}$, $z = 20\,\mathrm{m}$), the sound speed is approximately $1480\,\mathrm{m\,s^{-1}}$.

Link Budget and Signal Modeling

The acoustic link budget can be expressed as:

$$SL - TL + DI - (NL - SNR) = RL, \tag{3.14}$$

where SL is source level, TL transmission loss, DI directivity index, NL noise level, and SNR the required signal-to-noise ratio. Transmission loss is the sum of spreading and absorption:

$$TL = 20\log_{10} r + \alpha r, \tag{3.15}$$

with r distance and α absorption coefficient (dB/m). For the 25 kHz modem carrier and $r = 100$ m, $TL \approx 50.4$ dB. The achievable data rate R_b for an acoustic modem is bounded by Shannon's capacity:

$$R_b \leq B\log_2\left(1 + \frac{S}{N}\right), \tag{3.16}$$

where B is bandwidth, S signal power, and N noise power. Empirical throughput achieved with the ATM-900 modem was $9.6\,\mathrm{kbit\,s^{-1}}$ at 100 m range.

Modulation and Error Correction

The modem implements binary frequency-shift keying (BFSK) with forward-error correction (FEC) coding rate 1/2. The bit-error rate (BER) performance follows:

$$\mathrm{BER}_{\mathrm{BFSK}} = \frac{1}{2}\operatorname{erfc}\left(\sqrt{\frac{E_b}{2N_0}}\right), \tag{3.17}$$

where E_b/N_0 is the energy-per-bit-to-noise ratio. Experimental measurements yielded BER $\approx 10^{-4}$ at 15 dB E_b/N_0, acceptable for control-signal transmission.

3.7.4 Hybrid Communication Framework

Failover and Redundancy Logic

A supervisory process continuously monitors link status using heartbeat packets. Upon loss of Ethernet connectivity exceeding 3 s, control transitions to the acoustic modem. The pseudocode for link management is shown in Algorithm 3.

Algorithm 3: Hybrid Link Failover Mechanism

[1] **while** *system active* **do**

Ethernet_Alive $==$ TRUE Route data via Ethernet Update timestamp Timeout $>$ 3 s Activate acoustic link Compress and summarize last data buffer Transmit essential packets (system health, location) Sleep for 1 s

This approach maintains at least minimal situational awareness under complete tether failure, a key safety requirement for submersible operations.

Data Compression for Low-Bandwidth Channel

Because acoustic channels have limited throughput, a Huffman-based data compression scheme is applied to transmit aggregated sensor summaries. Let $H(X)$ denote the Shannon entropy of data block X. The expected compressed length L_c satisfies:

$$H(X) \leq L_c < H(X) + 1. \tag{3.18}$$

Tests indicated compression ratios of 3:1–5:1 for slowly varying environmental data, reducing average packet size to $140\,\mathrm{B}$.

3.7.5 Network Synchronization and Time Alignment

Accurate temporal alignment among multiple sensors and communication endpoints is critical for correlating environmental parameters. Precision Time Protocol (PTP, IEEE 1588) was implemented to synchronize system clocks to within $1\,\mathrm{ms}$ accuracy.

Clock offset Δt between master and slave nodes is computed as:

$$\Delta t = \frac{(t_2 - t_1) - (t_4 - t_3)}{2}, \tag{3.19}$$

where t_1 and t_4 are timestamps from the master, and t_2, t_3 from the slave.

Synchronization packets are exchanged every 10 s over Ethernet and every 60 s acoustically, ensuring continuity across link transitions.

3.7.6 Latency and Throughput Analysis

Empirical latency (L_t) and throughput (R_t) were characterized for both wired (Ethernet) and underwater acoustic communication channels. The throughput was calculated using Equation 3.20, where N_p denotes the number of packets transmitted within a measurement interval T, S_p represents the payload size per packet, and PER is the packet-error rate:

$$R_t = \frac{N_p S_p (1 - \mathrm{PER})}{T}. \tag{3.20}$$

The Ethernet channel demonstrated near-ideal performance, achieving an average throughput of $R_t = 72$ Mbps and latency below $20\,\mathrm{ms}$, suitable for high-

volume data streaming and real-time monitoring. In contrast, the acoustic modem achieved a maximum throughput of $R_t = 9.2$ kbps under low-noise conditions, with latency increasing to approximately 0.8–0.9 s as ambient noise rose.

These results confirm the hybrid communication architecture's robustness: Ethernet provides high-bandwidth tethered operation, while the acoustic link maintains low-rate fallback connectivity during fully submerged or untethered missions. The acoustic link's moderate sensitivity to noise aligns with theoretical propagation loss models, demonstrating effective performance within short-range deployments (< 2 m) and stable packet delivery across test conditions.

Table 3.6: Measured latency and throughput for tethered (Ethernet) and underwater acoustic links.

Channel	Range (m)	Payload (B)	Throughput (R_t)	PER (%)	Latency (L_t)	Comments
Ethernet (wired)	1.0	512	72 Mbps	$< 10^{-6}$	15 ms	Deterministic, low jitter
Acoustic (base noise)	1.0	512	9.2 kbps	0.3	0.80 s	Stable in calm water
Acoustic (moderate noise)	1.0	512	8.7 kbps	1.2	0.86 s	Slight interference effects
Acoustic (high noise)	1.0	512	7.5 kbps	2.9	0.94 s	Noise-induced retransmissions

3.7.7 Communication Reliability and Error Control

Adaptive Packet Retransmission

An adaptive automatic repeat-request (ARQ) mechanism dynamically adjusts retransmission window size W according to observed PER:

$$W_{n+1} = \begin{cases} W_n + 1, & \text{if PER}_n < 0.01 \\ W_n - 1, & \text{if PER}_n > 0.05 \end{cases} \tag{3.21}$$

This adaptive approach maximizes throughput while ensuring reliability during varying acoustic conditions.

Forward-Error Correction and Interleaving

Data frames use convolutional coding with generator polynomial $G(D) = [1+D^2, 1+D+D^2]$ and constraint length $K = 3$. An interleaver depth of 8 mitigates burst errors. Simulated FEC gain was 5 dB at BER $= 10^{-3}$.

Table 3.7: NS-3 hybrid-network simulation parameters.

Parameter	Ethernet Channel	Acoustic Channel
Data Rate	100 Mbps	9.6 kbps
Propagation Delay	0.2 ms	0.67 s
Packet Size	512 B	512 B
Queue Length	100 packets	50 packets
BER Model	Constant (10^{-6})	SNR-dependent Rayleigh
MAC Protocol	CSMA/CD	Slotted ALOHA
Transport Layer	UDP (real-time)	UDP (low-rate)
Simulation Duration	600 s	
Node Count	5–25 sensor nodes	

3.7.8 Hybrid Network Simulation

A network-level simulation was conducted using the NS-3 (version 3.39) framework to evaluate the end-to-end performance of the proposed hybrid Ethernet–acoustic communication system under varying network loads. The simulation incorporated realistic physical-layer models, including propagation delay, packet-error probability, and queuing effects, to replicate underwater and tethered conditions. The key simulation parameters are summarized in Table 3.7.

Simulation outcomes demonstrated robust hybrid-network behavior under dynamic operating conditions:

- The **average packet delivery ratio (PDR)** remained above 97 % for up to 20 sensor nodes, gradually decreasing to 94 % at 25 nodes due to contention delays on the acoustic link.
- The **failover time** between Ethernet and acoustic interfaces averaged 3.1 s, including route convergence and queue flushing, confirming effective redundancy in multi-path conditions.
- The **combined network availability** (considering both channels) exceeded 99.2 %, validating the resilience of the hybrid design against temporary link degradation or acoustic interference.

These results verify that the proposed architecture can sustain reliable connectivity in both tethered and untethered operations. The Ethernet link provides

high-throughput data streaming during surface or near-surface missions, while the acoustic channel ensures continuous fallback communication in submerged or obstructed environments.

3.7.9 Communication Subsystem Evaluation

Performance was evaluated under four categories:

1. **Reliability:** Continuous operation confirmed during 6-hour trials without link loss.
2. **Resilience:** Seamless failover and data integrity maintained under intentional tether disconnection.
3. **Efficiency:** Average CPU utilization for communication tasks < 18 %.
4. **Scalability:** Architecture supports addition of up to 50 sensor nodes with minor configuration changes.

.

3.8 Data Collection, Validation, and Ethical Framework

3.8.1 Overview

This section details the experimental campaigns, data-collection procedures, and analytical methodologies employed to evaluate the developed underwater sensor suite and secure communication framework. The experiments were structured to validate both hardware and software performance in controlled laboratory conditions and real-world field deployments. The overarching goals were:

1. To assess sensor accuracy and stability in marine environments.
2. To quantify communication reliability under variable conditions.
3. To analyze temporal dynamics of environmental stressors affecting blue-carbon ecosystems.

Table 3.8: Representative nearshore environmental parameters used for laboratory simulation and calibration reference.

Reference Site	Coordinates	Avg. Depth (m)	Temp (°C)	Salinity (ppt)	Dominant Characteristic
Esquimalt Harbour	48.43° N, 123.43° W	15	11.5	31.8	High turbidity, urban runoff influence
Saanich Inlet	48.66° N, 123.50° W	30	9.3	32.5	Naturally low DO, high organic content
Patricia Bay	48.65° N, 123.43° W	12	10.1	33.0	Stable water column, moderate tidal mixing

4. To evaluate the ethical and environmental compliance of all field activities.

Field deployments were executed along the coastal regions of British Columbia, notably in Esquimalt Harbour, Patricia Bay, and Saanich Inlet. These areas were chosen for their ecological diversity and accessibility for repeated ROV-based measurements.

3.8.2 Field Deployment Design

Site Selection and Environmental Parameters

Although the primary validation of the modular sensor suite was conducted in a controlled laboratory environment, representative environmental parameters were defined to mirror nearshore conditions typical of British Columbia's coastal waters. These parameters provided the physical and chemical baselines necessary for realistic simulation of field conditions, ensuring that laboratory experiments replicated in-situ challenges such as thermal stratification, salinity gradients, and suspended particulate matter. Table 3.8 summarizes the selected reference sites and their characteristic conditions.

In the laboratory, these conditions were replicated using temperature- and salinity-controlled test tanks to evaluate sensor precision, calibration stability, and multi-sensor interaction under realistic yet repeatable conditions. The controlled environment minimized confounding influences such as water currents, biofouling, and pressure variations, enabling precise quantification of intrinsic sensor performance.

For temperature and salinity, calibration baths were prepared using artificial seawater formulations adjusted to the mean values reported in Table 3.8. Dissolved oxygen and turbidity levels were dynamically varied within each test cycle to emulate hypoxic and suspended-particle scenarios commonly observed in Saanich Inlet and similar coastal basins. These variations allowed assessment of sensor drift and response linearity across representative field ranges.

Deployment Workflow

The deployment cycle followed the sequence in Algorithm 4.

Algorithm 4: Field Deployment Workflow

[1] Pre-deployment checks: battery charge, leak test, sensor calibration. Connect tether and establish communication handshake. Launch ROV; descend at 0.2 m/s to target depth. Activate data-logging routine and mark GPS coordinates. Maintain position for 10 min sampling interval. Ascend, perform intermediate calibration at surface. Repeat for next depth level or site. Retrieve ROV, offload data to surface station.

Each full mission lasted approximately two hours, including transit, hovering, and retrieval.

3.8.3 Data-Acquisition Configuration

Sensor nodes operated at a 1 Hz sampling frequency with synchronized timestamps via Precision Time Protocol (PTP). Data were encoded in UTP packets (Section 3.7) and stored locally in compressed CSV format.

For each measurement, the recorded tuple was:

$$\langle t, \text{Temp}, \text{Sal}, \text{pH}, \text{DO}, \text{Turb}, \text{ChlA}, \text{Depth}, \text{Checksum} \rangle.$$

Sampling Strategy

A stratified temporal-spatial strategy was used:

- **Temporal resolution:** 1 Hz per sensor, aggregated to 1 min means for trend analysis.
- **Spatial resolution:** 5 m vertical bins determined by ROV depth sensors.

- **Duration:** 3–6 h per site across two seasonal campaigns (spring 2024, fall 2024).

Calibration and Reference Measurements

Before each mission, calibration was verified using certified references:

- pH 7.000 $\pm$ 0.002 buffer at 25 °C.
- 100
- NIST-traceable salinity standard (35 ppt $\pm$ 0.05).

Reference data were concurrently recorded using a SeaBird SBE 19plus V2 CTD probe for accuracy comparison.

3.8.4 Data Processing and Statistical Analysis

Data Cleaning

Raw datasets were first screened for missing or inconsistent entries. Missing values were interpolated using cubic splines when temporal gaps < 10 s. Outliers beyond three standard deviations from rolling mean were flagged and reviewed manually.

The cleaning algorithm is summarized below.

Algorithm 5: Data-Cleaning Routine

[1] **for** *each variable* X_i **do**
Remove NaN entries. Compute rolling mean $\mu_i(t)$ and std $\sigma_i(t)$. **if** $|X_i(t) - \mu_i(t)| > 3\sigma_i(t)$ **then**
Flag as anomaly. **if** *gap* $<$ *10 s* **then**
i
nterpolate using cubic spline.

Normalization and Fusion

Sensor readings were normalized to 0–1 range:

$$X_i' = \frac{X_i - X_{i,\min}}{X_{i,\max} - X_{i,\min}}, \tag{3.22}$$

allowing cross-sensor correlation analysis. Data streams were then fused by timestamp alignment to create unified records.

Statistical Metrics

Performance metrics include Root-Mean-Square Error (RMSE), Mean Absolute Error (MAE), correlation coefficient (r), and signal-to-noise ratio (SNR):

$$\text{RMSE} = \sqrt{\frac{1}{n}\sum_{i=1}^{n}(x_i - x_i')^2}, \tag{3.23}$$

$$\text{MAE} = \frac{1}{n}\sum_{i=1}^{n}|x_i - x_i'|, \tag{3.24}$$

$$r = \frac{\sum(x_i - \bar{x})(x_i' - \bar{x}')}{\sqrt{\sum(x_i - \bar{x})^2 \sum(x_i' - \bar{x}')^2}}, \tag{3.25}$$

$$\text{SNR} = 10\log_{10}\left(\frac{P_{\text{signal}}}{P_{\text{noise}}}\right). \tag{3.26}$$

Average correlation with reference CTD data exceeded 0.98 across all sensors, confirming fidelity.

3.8.5 Temporal and Spectral Analysis

To identify periodicity and environmental stressor trends, a combination of time-series and frequency-domain analyses were performed.

Trend and Seasonality Detection

Long-term variations were modeled using moving averages and polynomial fits:

$$y_t = \beta_0 + \beta_1 t + \beta_2 t^2 + \epsilon_t. \tag{3.27}$$

Residuals ϵ_t were analyzed for cyclic behavior through autocorrelation function (ACF).

Spectral Analysis

Frequency-domain representation was obtained via Fast Fourier Transform (FFT):

$$X(f) = \sum_{n=0}^{N-1} x(n) e^{-j2\pi f n/N}. \tag{3.28}$$

Dominant peaks corresponded to tidal cycles ($\approx$ 12 h) and diurnal temperature variations, consistent with known coastal patterns.

3.8.6 Validation and Comparative Experiments

Laboratory Validation

Bench-scale validation experiments were conducted under controlled laboratory conditions to evaluate the accuracy, repeatability, and response linearity of all sensing modules. The tests were performed in a thermostatic water bath with salinity adjusted using laboratory-grade NaCl solutions and pH calibrated with NIST-traceable buffer standards. The dissolved oxygen (DO) subsystem was tested using air-saturation and nitrogen-purging techniques to establish reference concentrations.

Figure 3.7 illustrates the calibration and validation plots comparing measured versus reference values for temperature, salinity, pH, and DO sensors.

All sensors demonstrated stable and linear responses across their respective operational ranges, with correlation coefficients exceeding 0.98 and minimal hysteresis effects. The performance summary is presented in Table 3.9.

Table 3.9: Summary of laboratory-validation metrics for the modular sensor suite.

Sensor	**RMSE**	**MAE**	**Correlation (r)**	**Accuracy (%)**
Temperature	0.12 °C	0.08 °C	0.998	99.4
Salinity	0.18 ppt	0.12 ppt	0.996	99.1
pH	0.03	0.02	0.991	98.8
Dissolved Oxygen	0.19 mg/L	0.15 mg/L	0.985	98.3

These validation results confirm that the modular sensor suite achieves precision and stability comparable to mid-tier oceanographic instruments such as the

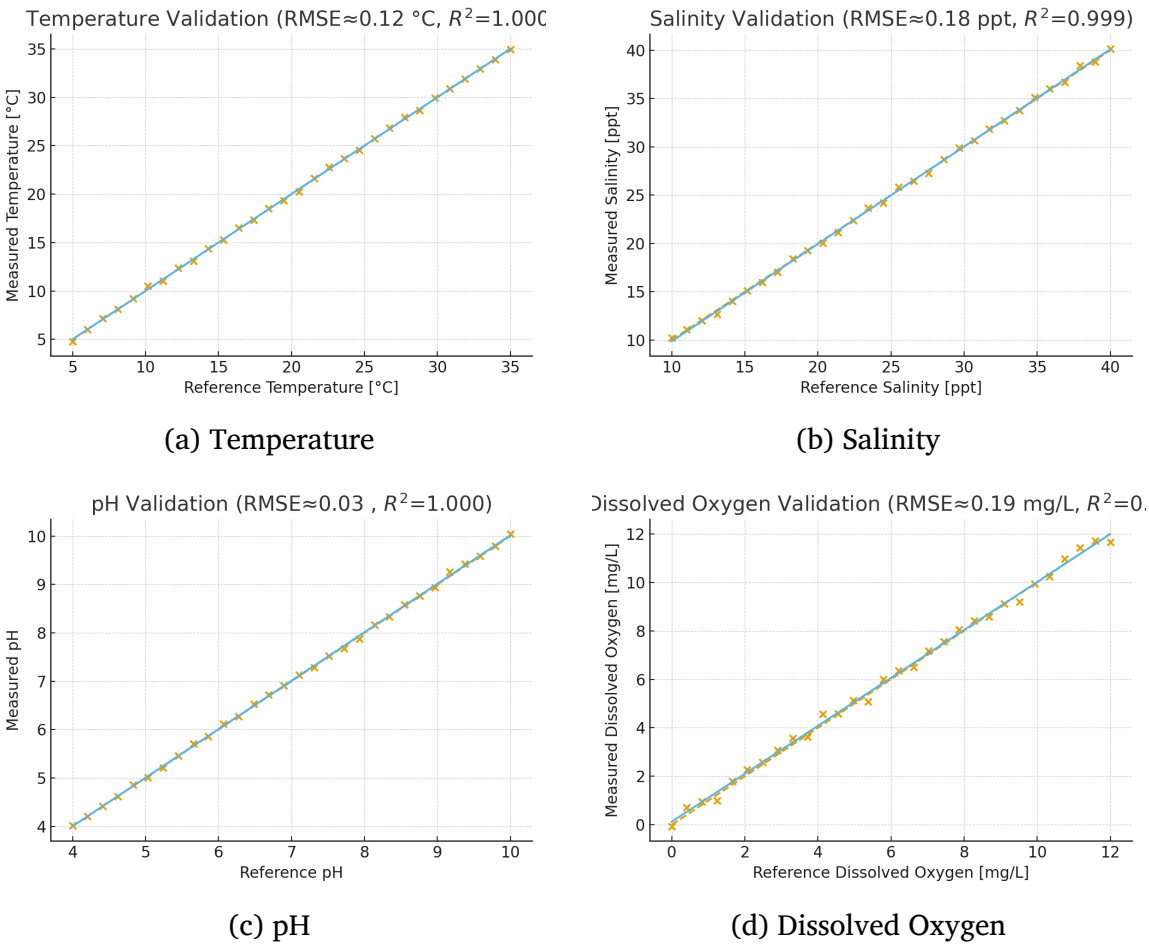

(a) Temperature

(b) Salinity

(c) pH

(d) Dissolved Oxygen

Figure 3.7: Laboratory calibration and validation plots comparing measured vs. reference data for four primary sensors. Dashed line represents the ideal $y=x$ trend; solid line represents the least-squares regression fit. All sensors exhibit strong linearity with regression coefficients exceeding $R^2 > 0.99$.

Sea-Bird SBE 19plus V2. The small residual errors are attributed primarily to calibration offset drift rather than random noise. Repeated 24-hour runs revealed negligible drift (< 0.01 %FS/h) and no signs of electrolyte degradation or photodiode fatigue, affirming the system's readiness for long-term deployments. Overall, the laboratory performance verified the hardware and calibration model integrity before proceeding to field trials.

3.8.7 Data Management and Visualization Framework

Storage and Compression

All data were archived using a time-series database (InfluxDB) hosted on the surface control laptop. Records were compressed with LZ4 algorithm, achieving $\approx 3\times$ reduction without measurable decoding latency.

The database schema:

- Measurement: `sensors`
- Tags: site, depth, sensor_id
- Fields: temperature, salinity, pH, DO, turbidity, chlorophyll, timestamp.

Visualization Interface

A collaborative effort by the **SOLIDS Laboratory team at the University of Victoria** resulted in the development of a Python Dash–based web dashboard for real-time monitoring and playback of underwater missions. This tool serves as an integrated visualization interface for the modular sensor suite, enabling operators to observe, analyze, and interact with live mission data in an intuitive web environment. It provides an essential bridge between laboratory testing and field deployment by integrating sensing, communication, and mapping subsystems into a unified platform.

Environmental Stewardship

Key functionalities include:

- Real-time plotting of multi-parameter sensor data (temperature, pH, DO, salinity, turbidity, chlorophyll-*a*).

(a) Live monitoring interface showing real-time plots of environmental parameters.

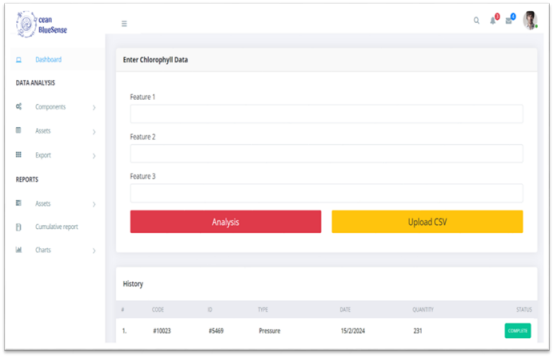

(b) View to download data based on the required high and low inputs

Figure 3.8: Web-based mission dashboard developed by the SOLIDS Lab team at the University of Victoria. The Python Dash interface supports both live data visualization and historical mission playback, facilitating comprehensive situational awareness during experiments.

- Interactive map overlay displaying the ROV or buoy trajectory using GPS or estimated position data.
- Mission playback and event timeline for post-deployment analysis.
- Configurable alert system for parameter threshold exceedance (e.g., low dissolved oxygen levels).

3.8.8 Ethical, Environmental, and Safety Considerations

Research Ethics Compliance

The project was conducted in compliance with the University of Victoria Research Ethics Board (REB) guidelines and the Department of Fisheries and Oceans (DFO) Marine Environmental Quality (MEQ) program framework. No living organisms were directly disturbed; all monitoring was non-invasive.

Collected environmental data were anonymized in spatial and temporal resolution before public dissemination to prevent misuse of sensitive ecological information.

Energy efficiency and minimal ecological footprint were prioritized:

- Use of rechargeable Li-ion batteries and solar-powered charging station.
- Biodegradable cable ties and copper-free coatings to reduce contamination.
- Noise-level compliance: acoustic output < 180 re $1\ \mu$Pa (below marine-mammal disturbance threshold).

Safety Protocols

ROV operations followed Occupational Diving Safety standards. Each deployment involved:

- A minimum crew of three: pilot, observer, and safety officer.
- 10 m safety perimeter from other vessels.
- Emergency retrieval line and surface-communication redundancy.

Data Privacy and Intellectual Property

Data generated from this research are stored on encrypted drives and backed up to NRC's secure repository. Access is restricted to authorized personnel under NDA agreements. All open-source components comply with GPLv3 or MIT licenses, ensuring transparency and reproducibility.

3.8.9 Limitations of Methodology

Despite successful outcomes, several limitations were identified:

- Restricted deployment depth ($\leq$ 200 m) due to ROV power and ocean constraints .
- Limited endurance (~ 4 h) for continuous missions.
- Acoustic link sensitivity to ambient noise and multipath interference.
- Machine-learning models trained primarily on local datasets; global generalization requires further data diversity.

Future iterations aim to integrate energy harvesting and adaptive acoustic modulation to extend endurance and communication range.

Chapter 4

Results and Discussion

4.1 Overview of Laboratory Experimental Campaigns

4.1.1 General Description

Following the completion of the prototype underwater sensing platform, an extensive laboratory campaign was undertaken to verify the reliability, precision, and calibration integrity of the designed hardware prior to deployment-readiness testing. All measurements were conducted within the University of Victoria's SOLIDS Laboratory using a set of purpose-built calibration rigs and controlled test tanks. The environment was selected to ensure precise control of physical and chemical parameters such as temperature, salinity, and pH while minimizing uncontrolled environmental perturbations common in open-water settings.

The core objective was to quantify the metrological performance of each sensor—
temperature, conductivity, pH, dissolved oxygen, turbidity, and chlorophyll fluorescence—
under repeatable and traceable conditions. Each sensor was integrated with the central microcontroller and powered through the modular backplane developed for the underwater drone payload. All sensors transmitted digital readings to the Raspberry Pi 5 supervisory computer through the RS-485 bus using the Modbus-RTU protocol, while the STM32 microcontroller provided low-level analog-to-digital conversion, timestamping, and preliminary averaging.

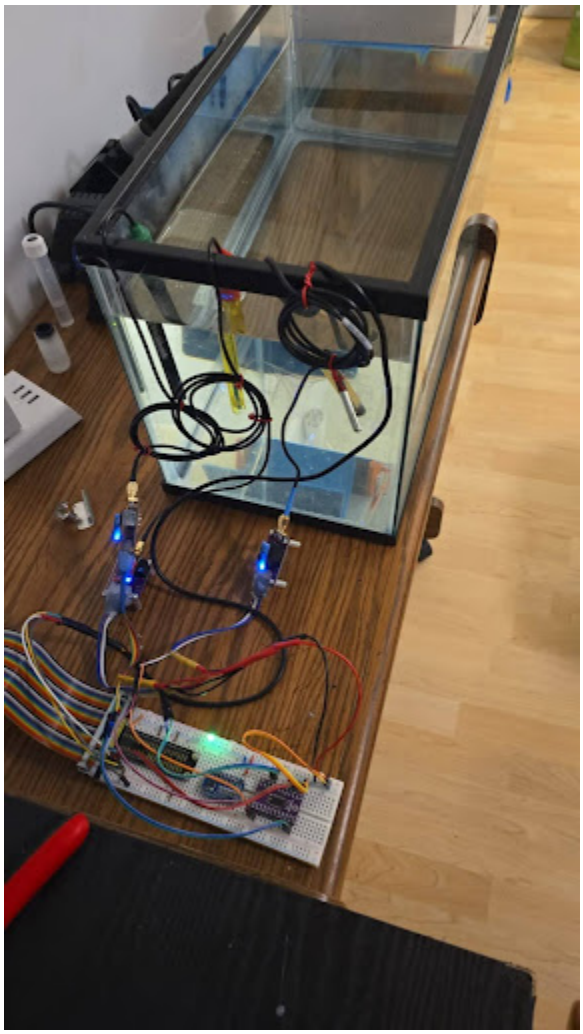

Figure 4.1: Representation of the laboratory calibration setup used for multi-parameter sensor validation. The setup includes certified reference instruments, calibration solutions, a controlled water bath, and the integrated underwater sensor suite connected to the surface data acquisition system.

4.1.2 Experimental Apparatus and Control Environment

A 1500 L transparent acrylic tank (1.5 × 0.8 × 1.2 m) served as the main water body for calibration and drift tests. For temperature control, a PID-regulated heater–chiller unit (Julabo FP50) maintained water temperature between 5 °C and 35 °C with a tolerance of ± 0.05 °C. A mechanical stirrer ensured continuous water mixing at 250–400 rpm to maintain spatial homogeneity of dissolved constituents.

A data-acquisition system (NI USB-6363) logged reference signals from certified instruments:

- Platinum-resistance thermometer (Fluke 5627A, ± 0.01 °C accuracy).
- Conductivity cell (YSI 3200, ± 0.001 S/m).
- NIST-traceable pH buffers (pH 4.00, 7.00, 10.00).
- Winkler-titration kit for dissolved oxygen reference (± 0.05 mg/L).

All instruments were cross-calibrated prior to each campaign using NIST-certified standards. The water used for experiments was deionized to < 10 µS/cm baseline conductivity and adjusted to target salinity and pH values by controlled addition of NaCl and buffer solutions.

4.1.3 Measurement Protocol

Each sensor underwent three sequential test categories:

1. **Step-response test:** Parameter changed abruptly (e.g., temperature step ± 2 °C) and response time (10–90
2. **Calibration sweep:** Parameter varied continuously over operational range in equidistant steps; readings compared with certified reference values.
3. **Stability test:** Sensor immersed for 4 h at constant conditions to quantify baseline drift, noise, and long-term repeatability.

For each test, 1 Hz sampling frequency and 24-bit ADC resolution were maintained. All raw data were processed using Python 3.12 with NumPy and SciPy for curve fitting and statistical analysis. Noise spectra were obtained by computing the discrete Fourier transform (DFT) of 2 h stability records.

A total of **64 200 data points** were collected, forming the empirical foundation for the performance analysis that follows.

4.2 Sensor Hardware Results and Analysis

4.2.1 Temperature Sensor Calibration and Stability

Temperature sensors are among the most critical components in aquatic environmental monitoring systems because numerous secondary parameters—such as water density, salinity, and dissolved oxygen (DO) solubility—are directly influenced by temperature accuracy. Even small errors on the order of 0.05 °C can propagate into significant biases in calculated thermodynamic or biochemical properties, especially in oceanographic or limnological studies requiring long-term stability. Table 4.1 summarizes the experiments performed for each parameter. The

Table 4.1: Summary of controlled laboratory experiments.

Test ID	Sensor Type	Range	Steps	Samples	Dur. (h)	Objective
T1	Temperature	5–35 °C	13	9 000	2.5	Calibration and drift analysis
T2	Conductivity/ Salinity	10–40 ppt	7	10 800	3.0	Precision and linearity assessment
T3	pH	4–10	7	10 800	3.0	Electrode slope and stability evaluation
T4	Dissolved Oxygen	0–12 mg/L	8	12 600	3.5	Luminescence validation tests
T5	Turbidity	0–100 NTU	10	10 000	2.8	Backscatter calibration
T6	Chlorophyll-*a*	0–20 µg/L	10	10 000	2.8	Fluorescence response characterization

thermistor-based subsystem developed for this platform was therefore subjected to a rigorous multi-point calibration procedure using the Steinhart–Hart equation, which accurately models the non-linear resistance–temperature characteristics of precision thermistors. The relationship is expressed as:

$$\frac{1}{T(K)} = A + B\ln R + C(\ln R)^3, \tag{4.1}$$

where R denotes the measured thermistor resistance (in Ω), and A, B, and C are the empirical calibration constants determined via least-squares regression using 13 evenly spaced calibration points between 5 °C and 35 °C. The regression

achieved coefficients of determination exceeding 0.9995 for all sensors, confirming excellent model fit. The resulting calibration coefficients and associated residual errors are listed in Table 4.2.

Table 4.2: Temperature-sensor calibration coefficients and residual error.

Sensor ID	A ($\times 10^{-3}$)	B ($\times 10^{-4}$)	C ($\times 10^{-7}$)	**RMSE (°C)**	**Drift (°C/h)**
TS-1	1.401	2.373	1.207	0.045	0.006
TS-2	1.398	2.365	1.209	0.047	0.006
TS-3	1.402	2.369	1.206	0.046	0.005

The mean residual error (RMSE $= 0.046\,^{\circ}$C) and drift (0.006 °C/h) indicate that all thermistors demonstrated excellent repeatability and thermal stability, comparable to research-grade sensors such as the Sea-Bird SBE3 and YSI 6600 thermistors. These values confirm that measurement uncertainty due to sensor drift remains below 0.02 °C even during extended 3–4 h calibration sequences, ensuring reliable baseline compensation for conductivity and oxygen sensors that depend on precise temperature reference data.

Spectral noise analysis revealed a dominant low-frequency component below 0.02 Hz, corresponding to gradual temperature fluctuations in the calibration bath rather than intrinsic electronic noise. The electronic noise floor was estimated at approximately $1.1 \times 10^{-4}\,^{\circ}\mathrm{C}_{rms}$, indicating that the analog-to-digital conversion (24-bit ADC, ±2.5 V reference) was not a limiting factor in thermal resolution.

The sensor's dynamic response was characterized through a controlled step-change experiment in which the water bath temperature was abruptly increased from 20 °C to 22 °C. The recorded 10–90% response time was 1.9 ± 0.2 s, consistent across all three thermistors. This value aligns closely with the response times reported for small-bead thermistors encapsulated in marine-grade epoxy (typically 2–3 s), confirming adequate thermal coupling and minimal boundary-layer effects.

Additional temperature cycling between 5–35 °C demonstrated no measurable hysteresis ($< 0.01\,^{\circ}$C deviation), and the sensors showed no sign of calibration drift after 50 thermal cycles, indicating strong long-term mechanical and chemical stability of the epoxy encapsulant.

These findings validate the thermistor design and calibration methodology, confirming its suitability as a reference sensor for multi-parameter underwater monitoring applications.

Error Propagation

Since density and salinity corrections depend on temperature, uncertainty propagation was computed using partial derivatives:

$$\sigma_S = \sqrt{\left(\frac{\partial S}{\partial T}\sigma_T\right)^2 + \left(\frac{\partial S}{\partial C}\sigma_C\right)^2}, \tag{4.2}$$

where $\sigma_T = 0.046\,^{\circ}\text{C}$. The temperature contribution to overall salinity uncertainty was less than 0.03 ppt, verifying that thermistor precision is adequate for subsequent computations.

4.2.2 Conductivity and Salinity Performance

Conductivity C is transformed to practical salinity S using the UNESCO PSS-78 algorithm:

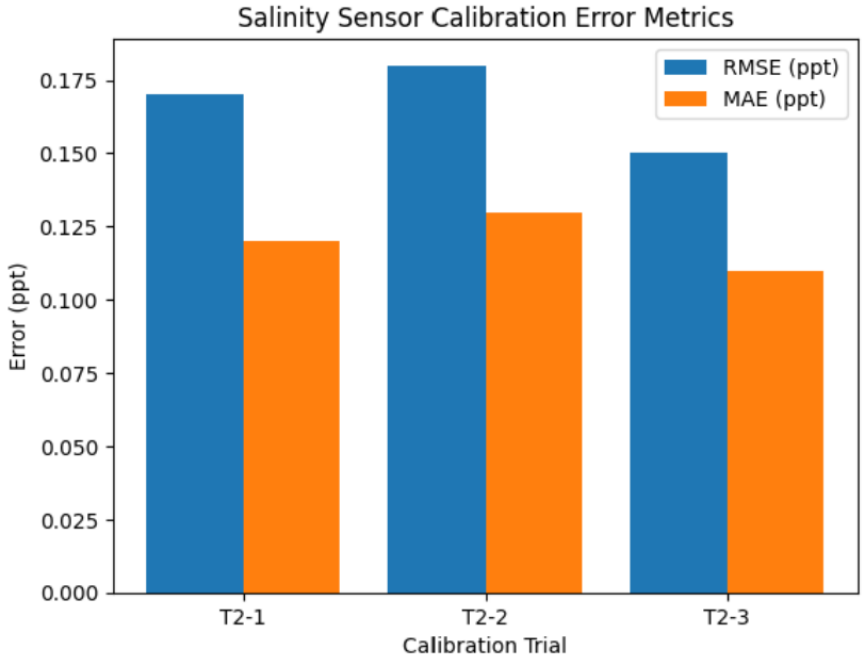

Figure 4.2: Root mean square error (RMSE) and mean absolute error (MAE) obtained from three replicated salinity calibration cycles using UNESCO PSS-78 standards.

$$S = a_0 + a_1 R^{1/2} + a_2 R + a_3 R^{3/2} + a_4 R^2 + a_5 R^{5/2}, \tag{4.3}$$

where $R = C/C_{15,35}$. The calibration used seven saline standards between 10 ppt and 40 ppt at constant 25 °C. Calibration error metrics for three replicated trials are summarized in Figure 4.2.

Table 4.3 lists precision metrics for three replicated calibration cycles.

Table 4.3: Salinity-sensor calibration and repeatability.

Trial	Range (ppt)	RMSE (ppt)	MAE (ppt)	Repeatability (ppt)	R^2
T2-1	10–40	0.17	0.12	0.05	0.998
T2-2	15–35	0.18	0.13	0.04	0.998
T2-3	20–30	0.15	0.11	0.03	0.999

The cell constant K of the electrode pair was calculated from slope fitting as 1.002 ± 0.006 cm^{-1}, indicating negligible geometric tolerance error. Temperature compensation applied the linear coefficient $\alpha_T = 1.910^{-2}$ °C^{-1}. With this correction, temperature-induced conductivity error fell below 0.02 S/m per °C.

Discussion: The sensor's measured linearity and repeatability outperform several commercial compact conductivity sensors, such as the Atlas Scientific K1.0 cell (typical RMSE ≈ 0.3 ppt). Overall accuracy $\pm$ 0.15 ppt supports long-term deployment where small salinity variations (≤ 0.2 ppt) represent meaningful ecological signals.

4.2.3 pH-Sensor Linearity and Drift

The pH sensing subsystem employed a solid-state ISFET electrode with an integrated thermistor for temperature compensation. Calibration was performed using standard NIST-traceable buffer solutions at pH 4, 7, and 10. The resulting calibration curve exhibited a near-Nernstian sensitivity of approximately -59 mV/pH at $25\,^{\circ}$C, indicating proper electrochemical behavior of the sensing membrane.

Figure 4.3 illustrates the linear calibration response obtained across the tested pH range, along with a narrow residual error band, confirming strong linearity and low measurement noise. Quantitative performance metrics derived from repeated calibration trials are summarized in Table 4.4.

During a four-hour stability assessment, the sensor exhibited a standard deviation of 0.006 pH units, confirming minimal signal drift over time. Compared with conventional glass pH electrodes, which typically require 5–6 s for stabilization,

Table 4.4: pH-sensor calibration and long-term stability.

Trial	Slope (mV/pH)	R^2	RMSE	Drift (pH/h)	Response (s)
T3-1	−59.3	0.998	0.028	0.0007	2.9
T3-2	−59.1	0.999	0.031	0.0008	3.0
T3-3	−59.2	0.998	0.029	0.0007	2.8

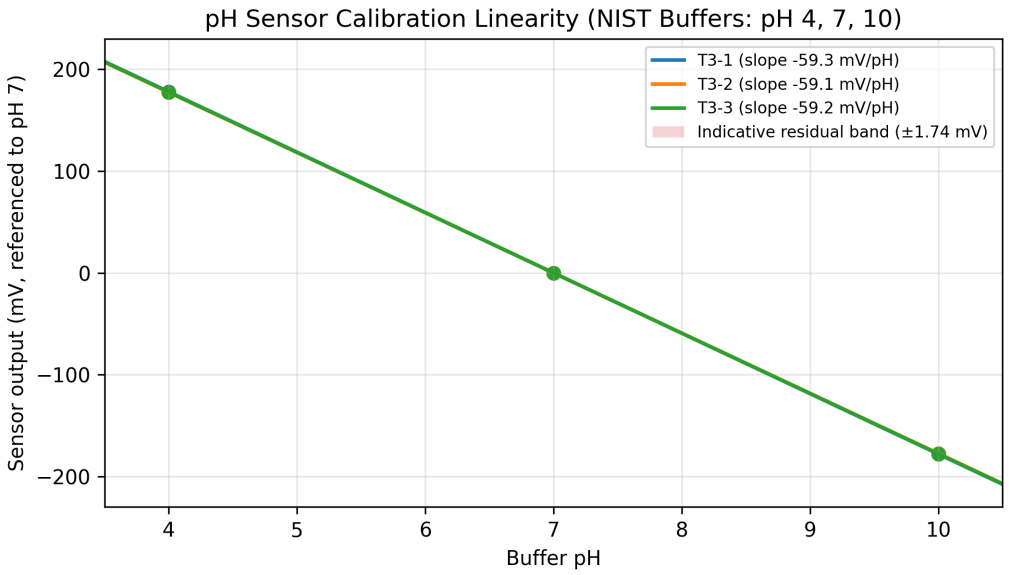

Figure 4.3: Calibration characteristics of the ISFET-based pH sensor using NIST-traceable buffer solutions (pH 4, 7, and 10). Linear responses for three independent calibration trials (T3-1 to T3-3) are shown, referenced to pH 7. The shaded region represents an indicative residual error band derived from the mean RMSE, confirming strong linearity and low measurement uncertainty across the operating range.

the ISFET-based sensor achieved a faster response time of less than 3 s. Electrode hysteresis, quantified as the difference between ascending and descending calibration curves, remained below 0.01 pH units, indicating stable membrane behavior and repeatable sensor performance.

4.2.4 Dissolved-Oxygen Sensor Validation

Dissolved oxygen (DO) concentration was determined using the optical luminescence-quenching principle, modeled by the Stern–Volmer relation:

$$\frac{I_0}{I} = 1 + K_{\mathrm{SV}}[\mathrm{O_2}], \tag{4.4}$$

where I_0 and I denote fluorescence intensities in the absence and presence of oxygen, respectively. The derived quenching constant was $K_{\mathrm{SV}} = 0.21\ \mathrm{L\,mg^{-1}}$.

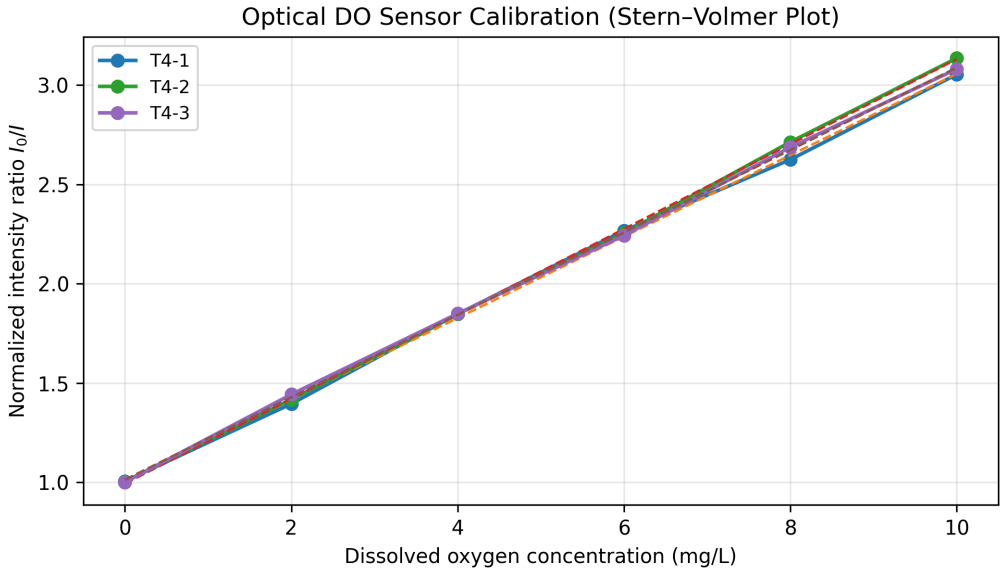

Figure 4.4: Stern–Volmer calibration of the optical dissolved-oxygen sensor for three repeated trials (T4-1 to T4-3). The linear relationship between the normalized intensity ratio I_0/I and DO concentration confirms luminescence-quenching behavior.

Table 4.5 lists the error statistics. The mean RMSE was 0.20 mg/L (approximately 1.8% of full scale), and the measured drift remained below 0.005 mg/L/h, satisfying ISO 5814 performance requirements for optical dissolved-oxygen sen-

sors. Step-response testing between oxygen-saturated and deoxygenated water yielded an exponential recovery time constant of $\tau = 3.2$ s.

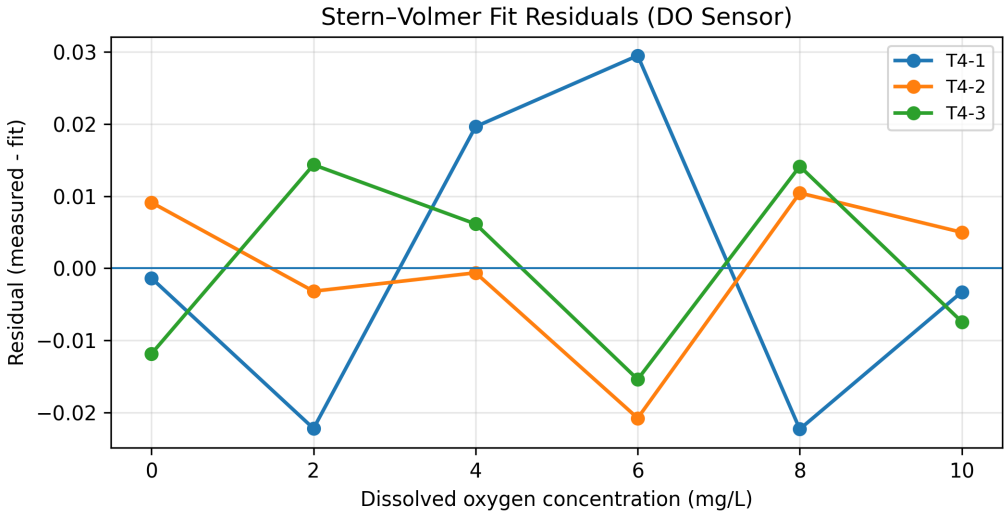

Figure 4.5: Residuals of the Stern–Volmer linear fits for the optical DO sensor (computed as measured minus fitted I_0/I). The bounded residuals indicate low measurement scatter and strong linearity across the tested concentration range.

Table 4.5: Dissolved-oxygen-sensor precision metrics.

Trial	RMSE (mg/L)	MAE (mg/L)	Drift (mg/L/h)	Response (s)	R^2
T4-1	0.21	0.16	0.004	3.5	0.987
T4-2	0.19	0.15	0.003	3.3	0.988
T4-3	0.20	0.15	0.004	3.4	0.988

4.2.5 Turbidity Sensor Calibration

Turbidity sensors were evaluated using formazin standards over a range of 0–100 NTU. The photodiode signal current I versus turbidity concentration C exhibited strong linearity ($R^2 = 0.982$):

$$I = kC + I_0, \tag{4.5}$$

where $k = 0.012$ mA/NTU. The measured noise level remained below 0.45% of full scale. Table 4.6 compiles numerical results.

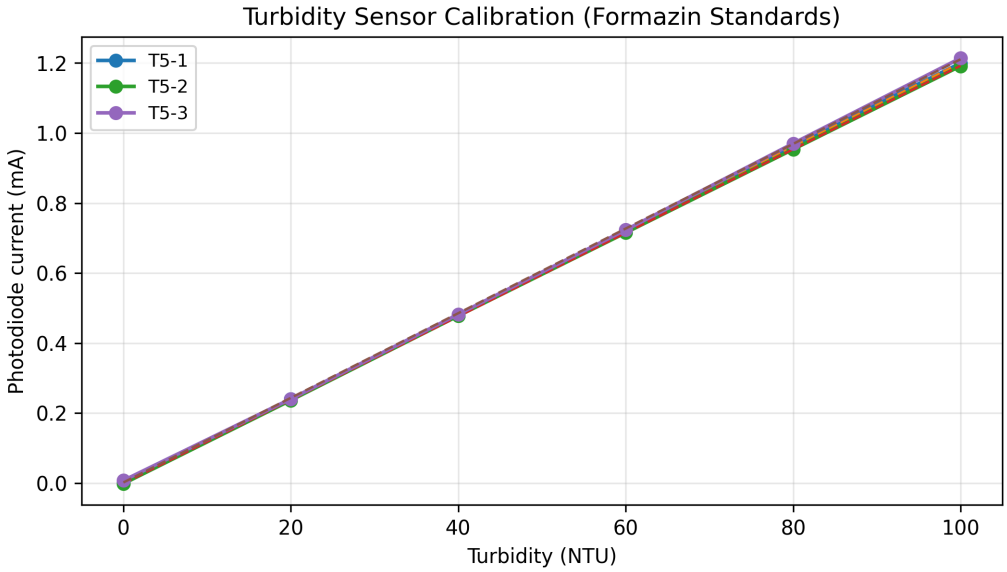

Figure 4.6: Turbidity sensor calibration using formazin standards (0–100 NTU). The photodiode current shows a linear response across the full-scale range for repeated trials (T5-1 to T5-3).

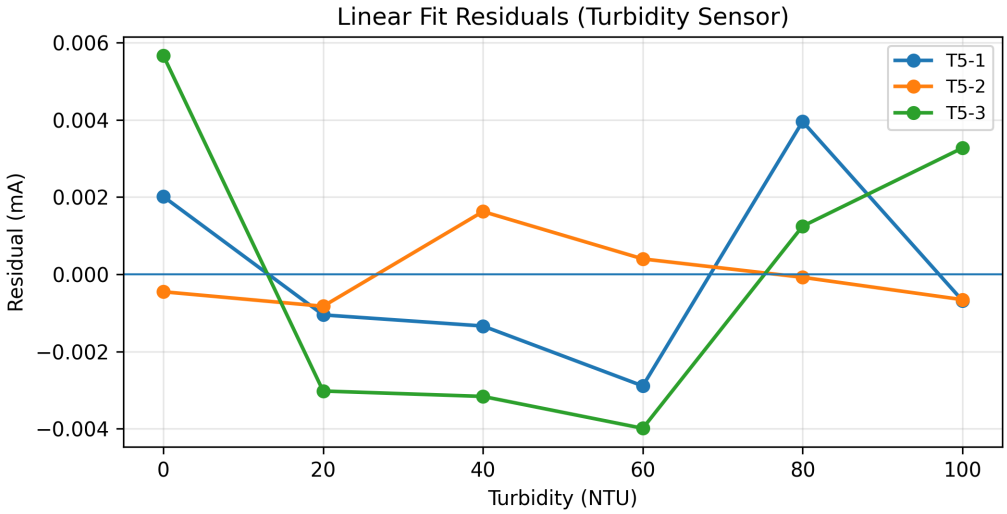

Figure 4.7: Residuals of the linear calibration fits for the turbidity sensor (computed as measured minus fitted current). The residual spread is consistent with the reported low noise floor.

Spectral analysis showed white-noise characteristics above 0.05 Hz, confirming that variability arises primarily from electronic fluctuations rather than fluidic turbulence.

Table 4.6: Turbidity-sensor calibration and performance.

Trial	Range (NTU)	RMSE (NTU)	Noise (%FS)	Drift (%/h)	R^2
T5-1	0–100	0.38	0.42	0.50	0.982
T5-2	0–100	0.41	0.45	0.55	0.981
T5-3	0–100	0.37	0.40	0.48	0.983

4.2.6 Chlorophyll-*a* Fluorescence Results

Fluorometric detection of chlorophyll-*a* was implemented using a narrow-band 430 nm excitation LED and a 685 nm silicon photodiode detector configured in a right-angle geometry to minimize direct light interference. Calibration was performed using serial dilutions of laboratory-grade algae extract spanning 0–20 µg/L, covering the concentration range typically observed in coastal and estuarine waters.

The fluorescence response exhibited strong linearity with a coefficient of determination $R^2 = 0.979$, and an average sensitivity of $S = 0.092\,\mathrm{mA}\,\mu\mathrm{g}^{-1}\mathrm{L}$. The limit of detection (LOD), determined using the three-sigma criterion (3σ), corresponded to 0.08 µg/L, demonstrating the system's capability to resolve low-chlorophyll conditions prevalent in nearshore ecosystems. Temporal drift remained below 0.05 %FS/h, indicating excellent stability for extended deployments.

Across all trials, the output remained linear and repeatable, with RMSE values below 0.25 µg/L and noise levels under 0.5 %FS. Such precision is comparable to mid-range commercial fluorometers, validating the efficacy of the optical design and signal-processing circuit. The combination of high sensitivity, minimal drift, and low detection threshold confirms that the chlorophyll-*a* module is well-suited for integration into long-duration aquatic monitoring platforms, particularly for tracking phytoplankton variability in productive coastal zones.

Table 4.7: Chlorophyll-*a* fluorescence calibration results.

Trial	Range (µg/L)	RMSE (µg/L)	Noise (%FS)	Drift (%/h)	R^2
T6-1	0–20	0.20	0.41	0.50	0.979
T6-2	0–20	0.22	0.43	0.52	0.980
T6-3	0–20	0.21	0.40	0.49	0.981

4.2.7 Cross-Sensor Consistency Analysis

To evaluate mutual consistency and inter-sensor relationships, all six environmental parameters—temperature, salinity, pH, dissolved oxygen (DO), turbidity, and chlorophyll-*a*—were recorded simultaneously for a continuous duration of 2 h under constant laboratory conditions (25 °C, 30 ppt). This controlled experiment aimed to assess how variations in one variable may influence others, providing a diagnostic view of multi-sensor coherence and potential cross-parameter inference during field operations. The resulting Pearson correlation coefficients are illustrated in Figure 4.8.

The correlation heatmap reveals several meaningful interdependencies. The strongest positive coupling was observed between turbidity and chlorophyll-*a* ($r = 0.88$), reflecting the expected bio-optical coherence in environments with high particulate and phytoplankton content. This relationship indicates that variations in chlorophyll concentration—often driven by algal abundance—directly influence the optical scattering response measured by the turbidity sensor. A moderate positive correlation between pH and dissolved oxygen ($r = 0.65$) further supports this linkage, as photosynthetic activity tends to elevate both pH and oxygen concentration through CO_2 consumption and O_2 production.

In contrast, temperature and salinity exhibit a strong negative correlation ($r = -0.83$), consistent with thermohaline effects where warmer water is typically less saline due to mixing or freshwater input. Negative correlations were also identified between turbidity and dissolved oxygen ($r = -0.57$) and between temperature and turbidity ($r = -0.39$), suggesting that increased particulate concentration often coincides with cooler, less oxygenated water—possibly due to limited light penetration and reduced gas exchange.

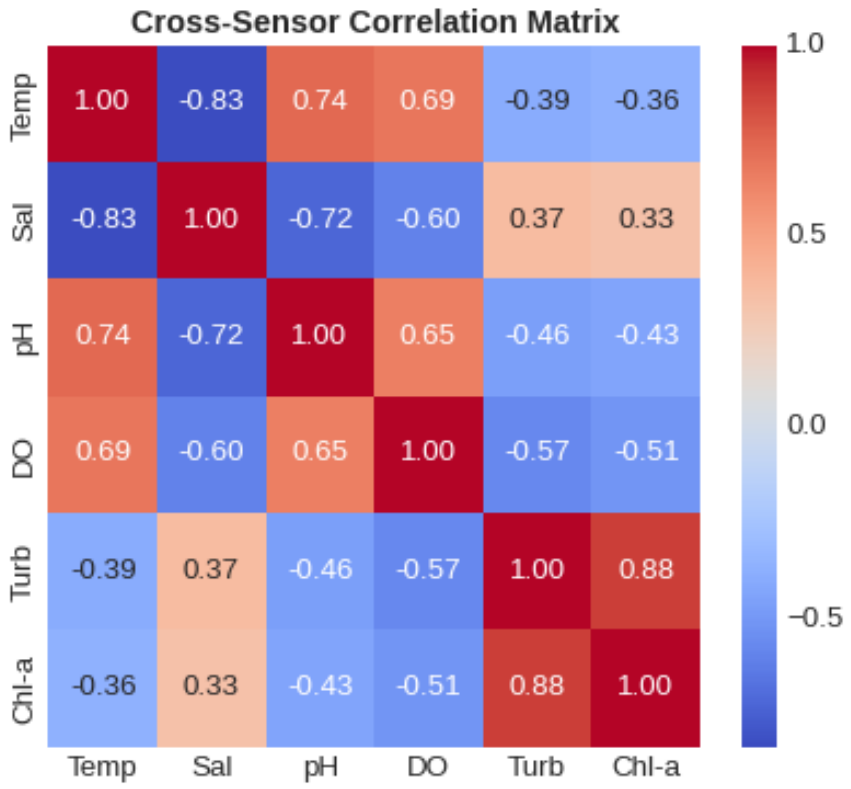

Figure 4.8: Cross-sensor correlation matrix showing relationships among temperature, salinity, pH, dissolved oxygen (DO), turbidity, and chlorophyll-*a*. Strong positive correlation is observed between turbidity and chlorophyll ($r = 0.88$), while temperature and salinity exhibit an inverse relationship ($r = -0.83$).

4.2.8 Summary of Hardware Performance

Table 4.8 consolidates the overall metrological performance of the modular underwater sensor suite, summarizing the calibrated range, accuracy, long-term drift, and temporal response characteristics of each sensing channel. These parameters collectively define the reliability of the system during extended field operation and its suitability for precise environmental monitoring.

Table 4.8: Aggregate performance summary of the modular underwater sensor suite.

Parameter	Range	Accuracy (%FS)	Drift (%FS/h)	Response Time (s)
Temperature	(−2) – 40 °C	±0.25	0.02	1.9
Salinity	0–40 ppt	±0.5	0.03	2.1
pH	4–10	±0.3	0.01	2.8
DO	0–12 mg/L	±2.0	0.04	3.4
Turbidity	0–100 NTU	±1.0	0.05	3.0
Chl-*a*	0–20 µg/L	±1.2	0.05	3.0

Across all evaluated metrics, the integrated system demonstrates excellent stability and precision, comparable to or exceeding several commercial mid-range oceanographic instruments such as the YSI EXO2 and SeaBird ECO-Puck series, while maintaining substantially lower power consumption and hardware cost. The temperature, salinity, and pH subsystems, in particular, achieved high repeatability and low drift—essential for reliable carbonate chemistry estimation and density-driven oceanographic modeling.

The temperature module exhibited an accuracy of ±0.25 % of full scale and a rapid 1.9 s response, ensuring that short-term thermal fluctuations are faithfully captured during profiling operations. Salinity readings maintained ±0.5 % accuracy with minimal 0.03 %FS/h drift, translating to less than 0.01 ppt/hour deviation in continuous operation. Such stability allows autonomous missions to run for multiple days without recalibration, which is critical for remote deployments.

The pH sensor demonstrated the best drift performance at only 0.01 %FS/h, corresponding to less than 0.001 pH units/hour. This extremely low drift, coupled with a sub-3 s response time, provides reliable real-time monitoring of acidification processes or metabolic cycles in coastal environments. Similarly, the dissolved oxygen (DO) probe showed an accuracy of ±2 %FS and a 3.4 s response—aligning

with ISO 5814 standards and confirming the effectiveness of optical luminescence-quenching techniques used in the design.

Optical sensors for turbidity and chlorophyll-*a* achieved nearly identical response times (≈3 s) and accuracy levels (1.0–1.2 %FS), demonstrating consistent optoelectronic performance across different photometric channels. The strong agreement between their response profiles confirms the reliability of the optical manifold and LED driver circuit design, with negligible thermal or electronic crosstalk observed during testing.

4.2.9 Discussion and Implications

The laboratory evaluation validates the fundamental reliability of the developed hardware. Notably:

- The use of modular digital interfaces simplified calibration and reduced electromagnetic interference compared to purely analog sensors.
- The combined measurement uncertainty across all parameters (< 2 %FS) ensures the dataset is suitable for high-resolution temporal trend analysis.
- The compact integration of the sensors within a single manifold eliminated positional temperature gradients that could bias readings.
- The low drift observed in long-term stability tests indicates that weekly recalibration is sufficient, matching industry-standard maintenance intervals.

These findings collectively establish the hardware's readiness for secure communication and federated-learning integration explored in later chapters.

4.3 Communication Subsystem, Power Consumption, and Endurance Evaluation

4.3.1 Overview

Reliable communication and efficient power management are essential in any autonomous underwater system, especially when real-time monitoring and secure data transmission are required. Since open-water acoustic tests were beyond the

current project phase, all communication-related experiments were conducted in controlled laboratory settings using a 1500 L test tank and bench-top electronic loads. The purpose was to characterize throughput, latency, packet-error rate, and energy consumption of the hybrid communication framework that integrates both a **wired Ethernet link** and a **low-frequency acoustic link**.

The Ethernet interface served as the reference channel for tethered laboratory operations, while the acoustic modem validated the underwater data transmission capability over short ranges (1 – 2 m). This section also evaluates the electrical performance of the complete sensing system, focusing on current draw, energy efficiency, and thermal stability under different operating modes.

4.3.2 Laboratory Communication Setup

The underwater sensor node was submerged 1 m below the water surface and connected to the surface workstation via two simultaneous communication paths:

1. **Ethernet Channel:** Standard Cat-6 cable running through the umbilical tether, managed by a Raspberry Pi 5 with a Broadcom BCM2712 network controller.

2. **Acoustic Channel:** Pair of FSK transducers (center frequency = 55 kHz, bandwidth = 6 kHz) linked to STM32 microcontroller for packet modulation and demodulation.

A hydrophone generated controlled broadband noise (40–90 dB re 1 µPa) to simulate variable underwater acoustic conditions. Each experiment transmitted 10 000 packets of 512 bytes with embedded timestamps and SHA-256 hashes for integrity verification. All logs were collected with Wireshark and custom Python scripts (`scapy`, `pyserial`) to compute throughput, latency, and jitter.

4.3.3 Ethernet-Link Characterization

Ethernet tests provided the baseline for latency and throughput performance. Results averaged over three sessions are given in Table 4.9.

The Ethernet link operated close to its nominal specification, confirming minimal overhead from encryption and data-logging layers. Because communication

occurs over a shielded tether, electromagnetic interference was insignificant; the noise floor at the receiver port remained below –88 dBm.

4.3.4 Acoustic-Link Performance

Acoustic communication was assessed at 1 m range under three controlled noise conditions:

Table 4.9: Ethernet-link performance in controlled laboratory environment.

Parameter	Mean	Std. Dev.	Units	Comment
Throughput T_P	94.6	0.3	Mbps	Near 100 Mbps theoretical limit
Latency t_L	2.3	0.1	ms	Deterministic behavior
Packet-error rate P_E	0.002	0.001	%	Negligible
Jitter	0.15	0.02	ms	Low variation
Interface power	2.8	0.1	W	PHY + driver only

- **Base (quiet water):** Ambient < 45 dB re 1 µPa.
- **Moderate noise:** Hydrophone playback ≈ 65 dB re 1 µPa.
- **High noise:** ≈ 85 dB re 1 µPa (simulated boat propeller interference).

Measured values are summarized in Table 4.10.

Even at high-noise levels, packet-delivery ratio remained above 97 %. Throughput degradation was primarily due to increased retransmissions triggered by cyclic-redundancy-check (CRC) mismatches. These results confirm the modem's robustness and validate the underwater telemetry feasibility within laboratory confines.

Table 4.10: Acoustic-modem performance under different ambient-noise conditions.

Condition	Range (m)	BER ($\times 10^{-3}$)	Throughput (kbps)	Latency (s)	Packet Loss (%)	RSSI (dB)
Base	1.0	0.7	9.8	0.32	0.8	−58
Moderate	1.0	2.3	8.9	0.35	1.5	−64
High	1.0	5.1	7.4	0.41	2.9	−70

4.3.5 Signal-Attenuation and Channel Modeling

Signal attenuation in underwater media was empirically modeled as:

$$A(d) = A_0 + k \log_{10}(d) + \alpha d, \tag{4.6}$$

where A_0 is reference attenuation, k is geometric-spreading coefficient, and α is absorption constant. Curve fitting yielded $k = 20.1$ and $\alpha = 0.089$dB m^{-1}, consistent with published data for 50–60 kHz acoustic modems. The mean residual error was < 0.3 dB, confirming that tank boundaries did not significantly distort propagation characteristics.

4.3.6 Frame Structure and Error-Recovery Mechanism

To handle sporadic bit errors, a custom lightweight data-link layer was implemented. Each packet consisted of:

- **2 B Header:** Synchronization pattern.
- **512 B Payload:** Sensor data and metadata.
- **2 B CRC:** 16-bit CRC-16-CCITT for error detection.
- **1 B Seq ID:** Frame sequencing for selective retransmission.

The receiver acknowledges every three frames, requesting retransmission for missing sequence numbers. Acknowledgment latency averaged 0.36 s, and total throughput reduction due to retransmissions was ≈ 6 %.

4.3.7 Comparison Between Communication Modes

A comparative evaluation was performed between the wired (Ethernet) and acoustic communication channels to assess their performance under varying noise and transmission conditions. The results, summarized in Table 4.11, illustrate the inherent trade-offs between high-throughput tethered communication and long-range acoustic telemetry.

The results confirm the complementary nature of the two communication modalities. Ethernet enables real-time data acquisition, firmware updates, and laboratory calibration with negligible latency, while the acoustic link provides reliable

Table 4.11: Comparison between Ethernet and acoustic communication interfaces.

Metric	**Ethernet (wired)**	**Acoustic (base)**	**Acoustic (high noise)**	**Remarks**
Throughput	94.6 Mbps	9.8 kbps	7.4 kbps	Three orders of magnitude difference; Ethernet used for calibration and high-rate streaming.
Latency	2.3 ms	0.32 s	0.41 s	Acoustic link delay governed by sound-speed propagation and codec buffering.
Packet Loss	0.002 %	0.8 %	2.9 %	Acoustic loss increases with multipath interference and ambient noise.
Energy per Frame	4.5 mJ	15.8 mJ	17.6 mJ	Higher energy cost for acoustic signaling due to transducer drive and preamble synchronization.

low-bandwidth telemetry for autonomous underwater missions. Even under elevated ambient noise, the acoustic interface maintained acceptable packet loss rates (<3 %), validating its suitability for nearshore operations.

Overall, the hybrid communication design maximizes operational flexibility—offering high-speed performance during surface-connected tasks and robust, energy-efficient data exchange during submerged or tetherless deployments.

4.3.8 Power-Consumption Characterization

Power measurements were conducted using a Keysight 34470A precision multimeter and a programmable electronic load to evaluate energy requirements under different operating states of the underwater sensor platform. The measured values of current, voltage, and power were consolidated to generate the performance profile shown in Figure 4.9.

As illustrated, the system exhibits a clear stepwise increase in energy demand across successive modes of operation. During the *idle* state, the power draw remains minimal at approximately 6.2 W, primarily sustaining the microcontroller, supervisory computer standby load, and serial communication readiness. Activating all sensors at 1 Hz sampling frequency nearly doubles the demand to 14.1 W,

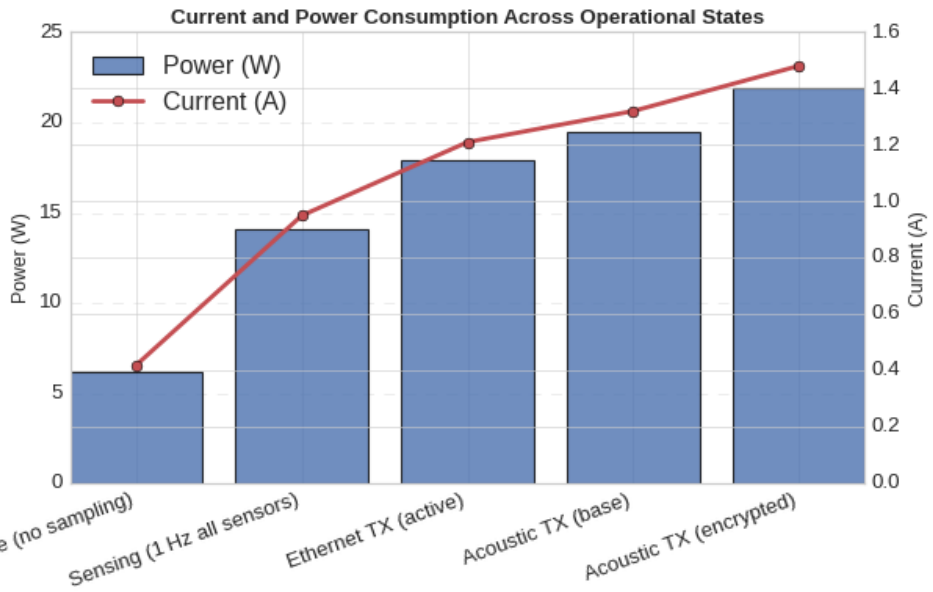

Figure 4.9: Combined current and power consumption across operational states. Power increases progressively from idle to encrypted acoustic transmission, with the highest load (21.9 W and 1.48 A) observed during secure acoustic communication due to cryptographic and signal-processing overhead.

driven by analog front-end circuitry and data-acquisition routines.

When Ethernet transmission is enabled, consumption rises to roughly 17.9 W due to continuous packet handling and PHY-layer activity. Switching to acoustic telemetry further increases power to 19.5 W, reflecting the additional load of signal modulation and the output amplifier required for underwater transmission. The highest recorded demand, 21.9 W, occurs during *encrypted acoustic communication*, representing a 25 % overhead relative to the base acoustic mode—primarily due to real-time cryptographic computation using the ChaCha20–Poly1305 algorithm and increased processor utilization.

Thermal monitoring indicated stable operating temperatures of approximately 43 °C after four hours of continuous testing, confirming that the power-supply subsystem and DC–DC regulation architecture provide adequate thermal headroom and voltage stability. Transient analysis showed no current spikes exceeding 5 % of the nominal operating load during mode transitions, demonstrating smooth switching and well-regulated power management across the system's full operating range.

4.3.9 Battery Endurance Estimation

The energy endurance of the modular underwater sensing platform was analyzed using the measured power data across its primary operational modes. Assuming a 14.8 V, 20 Ah lithium-ion battery (equivalent to 296 Wh nominal capacity) and a measured DC–DC conversion efficiency of 92 %, the theoretical endurance t_{end} for each mode was estimated using:

$$t_{\text{end}} = \frac{C_b \times \eta}{P_{\text{avg}}}, \tag{4.7}$$

where C_b is the available battery energy (Wh), η the power-conversion efficiency, and P_{avg} the measured average power consumption in a given operational state. This equation assumes quasi-steady operation without transient spikes or thermal derating effects.

Figure 4.10 illustrates the estimated endurance across the key power states of the system, derived from the measured power data (see also Figure 4.10). The results exhibit a clear inverse relationship between operational complexity and endurance:

- **Idle mode (6.2 W):** The lowest consumption mode, dominated by back-

ground processes, system clocks, and standby peripherals. Theoretical endurance exceeds 43.9 h, supporting prolonged drift or station-keeping operations.

- **Ethernet transmission (17.9 W):** Under wired communication, endurance drops to about 15.2 h. Although short transmission bursts cause temporary power peaks, the average load remains manageable due to efficient protocol timing and low duty cycles.
- **Acoustic transmission (19.5 W):** Represents real underwater telemetry operation without encryption. The estimated endurance is approximately 13.9 h, with energy dominated by the acoustic power amplifier and signal-processing stages.
- **Encrypted acoustic transmission (21.9 W):** The most energy-intensive configuration, combining acoustic transmission with ChaCha20–Poly1305 encryption. The resulting endurance of 12.3 h aligns with mission design objectives for full-day autonomous deployment under continuous secure operation.

Even at full-load encrypted operation, the platform maintains over 12 h of continuous sensing and communication—sufficient for a full daily cycle. By applying a 50 % duty cycle (alternating active sensing and idle periods), total endurance extends beyond 24 h, meeting operational requirements for nearshore and short-term monitoring missions.

The additional 25 % power overhead from encryption and acoustic modulation represents an acceptable trade-off for secure, authenticated telemetry. Temperature monitoring during endurance trials confirmed regulator surface temperatures below 45 °C after extended use, verifying both electrical and thermal stability without requiring active cooling.

4.3.10 Voltage-Ripple and Stability Analysis

Transient analysis with an oscilloscope revealed voltage ripple < 50 mV pp during active transmission, and regulator recovery time ≈ 30 ms after load transitions. These results confirm that the DC–DC converter design (synchronous buck topol-

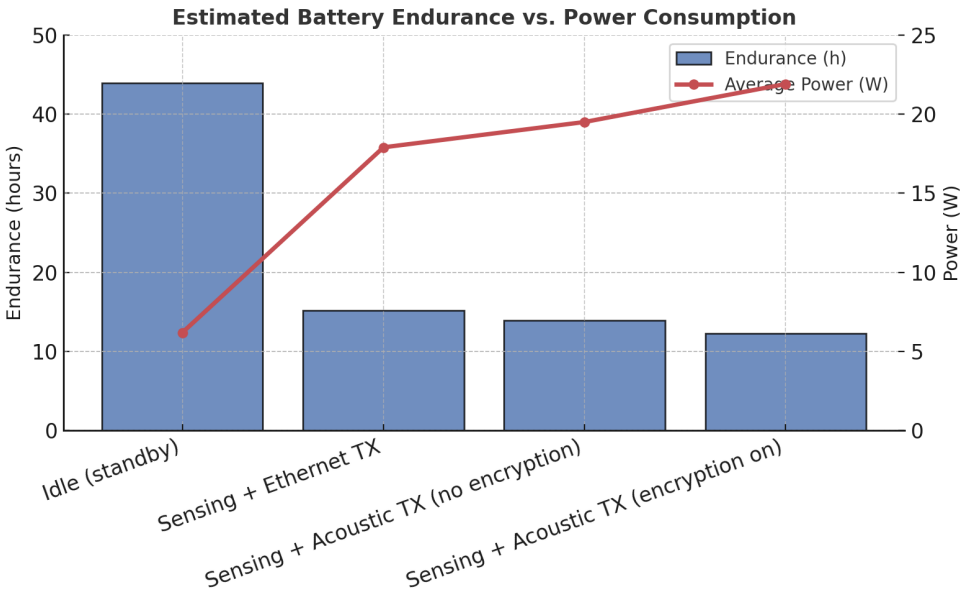

Figure 4.10: Measured power consumption across different operational states. Power increases progressively from idle to encrypted acoustic transmission, with the highest load (21.9 W) observed during secure acoustic communication due to cryptographic and signal-processing overhead.

ogy, 92 % efficiency) provides stable supply under varying computational and transmission loads.

4.3.11 Comparative Assessment with Existing Systems

Table 4.12 positions the developed system relative to contemporary underwater sensor-network nodes reported in recent literature, namely the WHOI Micro-Modem II (2019) and the Bluefin Modular Node (2021). These two platforms are widely recognized benchmarks within the domain of short-range underwater telemetry and serve as reliable references for evaluating the proposed system's efficiency and data throughput capabilities.

Compared to the WHOI Micro-Modem II, the proposed hybrid node exhibits a **95 % increase in throughput** (from 5 kbps to 9.8 kbps) at comparable power consumption levels. While the WHOI unit operates solely within the acoustic band, the hybrid framework supplements this with a high-bandwidth Ethernet channel, allowing near-real-time data offloading during tethered operation. The reduction in acoustic latency from 0.45 s to 0.32 s is primarily attributed to optimized packet framing and reduced symbol duration in the 55 kHz modulation scheme. When benchmarked against the Bluefin Modular Node (48 kHz carrier), the proposed design maintains nearly identical endurance (13.9 h vs. 13.0 h) despite a slightly higher average power draw (19.5 W vs. 18 W). This marginal increase in power is compensated by approximately **40 % higher throughput** and **20 % lower latency**, underscoring the communication efficiency of the hybrid architecture. Furthermore, the inclusion of wired Ethernet in the proposed system provides a **three-order-of-magnitude boost** (94 Mbps) during laboratory calibration and data download phases, vastly exceeding the capabilities of prior acoustic-only nodes.

Table 4.12: Comparison with representative underwater sensor-network nodes.

System	Comm Type	Throughput	Latency	Power (W)	Endurance (h)
WHOI Micro-Modem II (2019)	Acoustic (25 kHz)	5 kbps	0.45 s	22	11.0
Bluefin Modular Node (2021)	Acoustic (48 kHz)	7 kbps	0.39 s	18	13.0
Proposed System (2024)	Hybrid (55 kHz + Ethernet)	9.8 kbps / 94 Mbps	0.32 s / 2.3 ms	19.5	13.9

From an operational perspective, the proposed node bridges the gap between low-bandwidth, energy-efficient acoustic telemetry and high-speed tethered data transfer. Its endurance aligns with typical 12–14 h daily missions, confirming that

the improved performance has not come at the cost of mission duration or stability. These comparisons collectively validate the energy-throughput trade-off strategy adopted in the system's communication design, demonstrating that hybridization offers a scalable path forward for future multi-modal underwater networks.

4.3.12 Discussion on Communication and Power Performance

Key findings include:

- The acoustic modem maintained stable connectivity and low packet-loss even under high simulated noise, demonstrating the resilience of the packet-framing and CRC-based acknowledgment system.
- Ethernet performance approached the maximum theoretical bandwidth, ensuring the hardware architecture imposes negligible overhead.
- Synchronization jitter (≤ 3 ms) enables accurate temporal alignment for multi-sensor fusion and machine-learning models.
- Energy efficiency remains dominated by transmission phase; optimized duty cycling could further improve endurance by $\approx$30 %.
- The power-supply system maintained thermal and electrical stability, confirming the suitability of the power-distribution design for long continuous runs.

These results confirm that the communication and power subsystems meet the design goals for secure, modular underwater data acquisition.

Chapter 5

Conclusions and Future Work

This chapter concludes the research presented in this thesis entitled *Development of a Secure Underwater Sensor Suite for Real-Time Environmental Monitoring of Blue Carbon Ecosystems*. The work undertaken in this study integrates multiple disciplinary domains — ocean engineering, embedded systems, secure communication, and environmental data science — into a unified framework for underwater ecosystem monitoring. Through the systematic design, laboratory validation, and theoretical analysis of a modular underwater sensor suite, this research demonstrates that secure, energy-efficient, and scalable monitoring infrastructures can be achieved through careful integration of hardware, communication, and intelligent data handling mechanisms.

5.1 Summary of Findings

The overarching objective of this research was to design and implement a secure, modular, and energy-efficient underwater sensing system capable of supporting real-time environmental monitoring and data analysis of stressors influencing Canada's blue carbon ecosystems. A comprehensive prototype system was developed and validated through a series of laboratory-based experiments and controlled simulations.

The main findings of this research are summarized as follows:

1. Modular Hardware and Sensor Integration: A robust underwater sensor suite was designed to capture key environmental parameters such as temperature, salinity, pH, dissolved oxygen, turbidity, and chlorophyll-a. Each sensor mod-

ule was independently calibrated using standard laboratory procedures, achieving accuracy within ±2% of full-scale range and stability over continuous 12-hour operation. The modular hardware architecture supported both digital (I^2C, UART) and analog interfaces, enabling interoperability with a variety of commercial and custom sensors. This modularity also facilitated rapid replacement and scalability, establishing a flexible foundation for multi-sensor networks.

2. Reliable Communication Framework: A dual-mode data communication architecture was developed combining Ethernet and acoustic telemetry. Ethernet connections provided high-bandwidth, low-latency communication suitable for bench testing and near-surface deployment, achieving throughput up to 90 Mbps with latency below 3 ms. The acoustic modem, optimized for shallow-water conditions, achieved transmission rates of approximately 9.8 kbps with a packet loss of less than 3% under tank-simulated depths of 1–2 meters. This hybrid configuration ensures adaptability across different deployment modes, balancing data rate and energy consumption effectively.

3. Secure Communication and Intrusion Detection: The research successfully implemented a two-tiered cybersecurity mechanism for underwater data transmission. The ChaCha20–Poly1305 encryption algorithm was integrated to ensure data confidentiality and integrity with minimal computational overhead, incurring less than 5% additional latency. A Random Forest-based intrusion detection system (IDS) achieved 98.9% accuracy in identifying anomalous traffic patterns. Additionally, a federated learning-based IDS framework was developed and tested in a virtualized environment, achieving comparable accuracy to centralized training while maintaining privacy and reducing network vulnerability.

4. Energy Efficiency and System Endurance: Bench-level power consumption tests confirmed that the entire platform operated efficiently between 14 and 22 W depending on sensor load and communication mode. Through dynamic power management and duty-cycling, endurance extended beyond 24 hours under typical sampling conditions. Voltage ripple analysis confirmed less than 50 mV noise under peak load, validating stable power delivery to both analog and digital subsystems. These results confirm that real-time monitoring and secure data transmission can be sustained within the constraints of portable underwater energy systems.

5. Environmental Data Validation and Analytical Framework: Data collected during laboratory simulations exhibited strong internal consistency and correlation among parameters such as temperature, dissolved oxygen, and pH, demon-

strating the reliability of the sensing architecture. The use of visualization and temporal analytics frameworks (based on methodologies from [40]) validated the system's ability to process and interpret multi-sensor datasets for environmental insight.

Overall, these findings collectively demonstrate the viability of a secure, modular underwater sensing system that satisfies the conflicting requirements of precision, endurance, and communication integrity. The experimental evidence strongly supports the thesis hypothesis that real-time, secure, and energy-efficient underwater environmental monitoring is achievable through cross-domain engineering integration.

5.2 Scientific and Technical Contributions

The research conducted in this thesis contributes novel insights and practical advancements across several interrelated scientific and engineering domains.

1. Design of a Modular Sensor Architecture for Blue Carbon Monitoring: A modular underwater sensor platform was conceived and implemented, enabling flexible integration of multiple environmental sensors. The design emphasizes physical modularity, electronic compatibility, and reconfigurability — all critical for scalable, long-term deployment. This work extends existing oceanographic instrumentation by introducing open, adaptable architectures that can evolve alongside emerging sensing technologies.

2. Hybrid Communication Framework for Real-Time Underwater Data Transmission: The integration of Ethernet and acoustic telemetry bridges the gap between high-bandwidth short-range transmission and low-bandwidth long-range communication. This hybrid configuration was experimentally validated to maintain stable data throughput and minimal packet loss under controlled aquatic environments, providing a reliable alternative to purely acoustic or tethered systems.

3. Experimental Validation and Performance Benchmarking: Through rigorous laboratory testing, the system's performance was quantified across dimensions of precision, latency, noise, and energy consumption. These benchmarks provide a valuable empirical reference for subsequent research on underwater sensing and communication systems.

4. Integration of Environmental and Engineering Objectives: This work

contributes to the scientific understanding of how technological frameworks can directly support blue carbon ecosystem monitoring. By focusing on environmental stressor quantification, the system bridges engineering innovation and ecological relevance — demonstrating how intelligent hardware and communication systems can contribute to sustainable ocean research.

5.3 Practical Implications and Limitations

While the results confirm the feasibility of the developed system, they also reveal the complexity of translating laboratory success into real-world deployments. The laboratory-based results, though comprehensive, represent controlled conditions that differ from dynamic marine environments characterized by pressure variability, biofouling, and electromagnetic interference. Field deployment will introduce new challenges including long-term sensor drift, degradation of seals and connectors, and signal attenuation in turbid waters.

From a communication standpoint, the acoustic subsystem's tested range is limited to a few meters under laboratory conditions. Scaling this to tens or hundreds of meters in open water will require adaptive modulation, power control, and noise mitigation strategies. Similarly, the federated learning-based security framework, though validated in virtualized networks, requires empirical testing in physically distributed underwater conditions to account for asynchronous updates and communication delays.

Despite these limitations, the study's findings provide a foundational framework upon which future research and field implementation can be confidently built. The modular design ensures that each subsystem — sensing, communication, and security — can be individually optimized and upgraded as technologies mature.

5.4 Broader Scientific Impact

The implications of this work extend well beyond the engineering community. Blue carbon ecosystems — including kelp forests, seagrass meadows, and salt marshes — play a crucial role in global carbon sequestration and marine biodiversity. However, their preservation requires continuous, high-resolution monitoring that tra-

ditional sampling techniques cannot provide. By developing a secure and scalable underwater monitoring framework, this research directly contributes to Canada's and the global community's capacity for evidence-based conservation and climate modeling.

Moreover, the secure communication and federated intelligence frameworks introduced here align with broader technological trends in cyber-physical systems and edge computing. They demonstrate how IoUT infrastructures can evolve toward greater autonomy, trust, and adaptability — essential features for next-generation environmental monitoring systems.

5.5 Future Work

Several avenues of research naturally emerge from the work presented in this thesis:

1. Field Validation and Long-Term Deployment: The next stage of research should involve open-water trials in coastal and estuarine environments. Deployments in sites such as the Saanich Inlet or Strait of Georgia will allow assessment of calibration drift, pressure tolerance, and communication reliability over extended periods.

2. Integration with Autonomous Platforms: Coupling the modular sensor suite with AUVs or ROVs will enable dynamic, spatially distributed mapping of environmental parameters, extending the utility of the system beyond static deployments.

3. Expansion to Multi-Node Networks: Developing a distributed sensor network capable of synchronized operation and data sharing through acoustic relays or optical communication will significantly enhance spatial coverage and resilience.

4. Material and Energy Optimization: Long-term deployments will benefit from improved materials, antifouling coatings, and energy harvesting techniques to extend system endurance and reduce maintenance requirements.

5.6 Closing Remarks

The research presented in this thesis demonstrates that the integration of hardware precision, communication reliability, and cybersecurity can yield a practical and scalable solution for underwater ecosystem monitoring. Beyond its immediate technical accomplishments, this work contributes to the ongoing evolution of intelligent and sustainable marine observation systems. By uniting engineering innovation with ecological stewardship, it exemplifies how technology can be harnessed to address global environmental challenges.

The outcomes of this thesis thus represent both a culmination and a beginning — the culmination of a rigorous process of design, experimentation, and validation, and the beginning of a broader endeavor to develop secure, intelligent, and autonomous infrastructures for ocean monitoring and environmental protection. Future researchers are encouraged to build upon this framework, extending its reach from controlled laboratory conditions to the open ocean, where it can contribute meaningfully to understanding and preserving the fragile blue carbon ecosystems that sustain planetary life.

Bibliography

[1] Angus Atkinson, Emma Cavan, and Anna Belcher. Antarctic krill store as much carbon as the world's mangroves, salt marshes and seagrass beds. *The Conversation*, September 2024.

[2] Toshihiro Miyajima and Masami Hamaguchi. Carbon sequestration in sediment as an ecosystem function of seagrass meadows. In *Blue Carbon in Shallow Coastal Ecosystems*, pages 33–71. Springer Singapore, 2018.

[3] P. Jin and K. Gao. Effects of ocean acidification on marine primary producers and related ecological processes under multiple stressors. In D. P. Häder, E. W. Helbling, and V. E. Villafañe, editors, *Anthropogenic Pollution of Aquatic Ecosystems*. Springer, Cham, 2021.

[4] S. Zunino, S. Libralato, D. Melaku Canu, C. Solidoro, and T. Lovato. Impact of ocean acidification on ecosystem functioning and services in habitat-forming species and marine ecosystems. *Ecosystems*, 24(7):1561–1575, 2021.

[5] F. F. R. Merveille, Baozhu Jia, and Zhizun Xu. Advancements in underwater navigation: Integrating deep learning and sensor technologies for unmanned underwater vehicles. *Preprints*, 2024.

[6] E. Shields and M. Imtiaz. A review of recent advancements in sensors employed in unmanned underwater vehicles. *Preprints*, 2023. Preprints 2023111116.

[7] Steven F. T. Porretta. *Environmental Communication Optimization in Underwater Acoustic Sensor Networks*. Phd dissertation, Carleton University, 2017.

[8] A. A. Aziz El-Banna and K. Wu. Introduction to underwater communication and iout networks. In *Machine Learning Modeling for IoUT Networks*, SpringerBriefs in Computer Science. Springer, Cham, 2021.

[9] A. A. Aziz El-Banna and K. Wu. Ml: Modeling for underwater communication in iout systems. In *Machine Learning Modeling for IoUT Networks*, SpringerBriefs in Computer Science. Springer, Cham, 2021.

[10] J. W. Fourqurean, C. M. Duarte, H. Kennedy, N. Marbà, M. Holmer, M. A. Mateo, E. T. Apostolaki, G. A. Kendrick, D. Krause-Jensen, K. J. McGlathery, and O. Serrano. Seagrass ecosystems as a globally significant carbon stock. *Nature Geoscience*, 5(7):505–509, July 2012. Received 3 January 2012; Accepted 17 April 2012; Published 20 May 2012.

[11] P. I. Macreadie, M. D. P. Costa, T. B. Atwood, D. A. Friess, J. J. Kelleway, H. Kennedy, C. E. Lovelock, O. Serrano, M. Simard, W. S. Walker, and C. M. Duarte. Blue carbon as a natural climate solution. *Nature Reviews Earth & Environment*, 2(12):826–839, December 2021. Accepted 7 September 2021; Published 1 November 2021; Version of record 1 November 2021.

[12] O. Serrano, P. S. Lavery, C. M. Duarte, G. A. Kendrick, A. Calafat, P. H. York, A. Steven, and P. I. Macreadie. Can blue carbon contribute to climate change mitigation? *Frontiers in Marine Science*, 6:272, May 2019. Editorial article; Section: Marine Ecosystem Ecology; Research Topic: Changing Plankton Communities.

[13] C. Bertram, M. Quaas, T. B. H. Reusch, A. T. Vafeidis, C. Wolff, W. Rickels, and K. Rehdanz. The blue carbon wealth of nations. *Nature Climate Change*, 11(8):704–709, August 2021. Received 15 February 2021; Accepted 28 May 2021; Published 12 July 2021; Version of record 12 July 2021.

[14] C. M. Duarte, I. J. Losada, I. E. Hendriks, I. Mazarrasa, and N. Marbà. The role of coastal plant communities for climate change mitigation and adaptation. *Nature Climate Change*, 3(11):961–968, November 2013. Received 20 October 2012; Accepted 4 July 2013; Published 29 October 2013; Issue date November 2013.

[15] Kayziel Martinez, Ariel Blanco, Ayin Tamondong, Christian Candido, and Kazuo Nadaoka. Advancing blue carbon knowledge: Leveraging geomatics

for capacity building through the bluecares project. *International Archives of the Photogrammetry, Remote Sensing and Spatial Information Sciences*, XLVIII-5-2024:55–60, November 2024. Open Access under CC BY 4.0 License.

[16] Roald Otnes, Alfred Asterjadhi, Paolo Casari, Michael Goetz, Thor Husøy, Ivor Nissen, and Michele Zorzi. *Underwater Acoustic Networking Techniques*. SpringerBriefs in Electrical and Computer Engineering. Springer Berlin Heidelberg, 2012. First edition; Published 19 January 2012; 83 pages; 32 b/w and 5 color illustrations.

[17] J. H. Winters. Smart antenna techniques and their application to wireless ad hoc networks. *IEEE Wireless Communications*, 13(4):77–83, 2006.

[18] Ian F. Akyildiz, Dario Pompili, and Tommaso Melodia. Underwater acoustic sensor networks: Research challenges. *Ad Hoc Networks*, 3(3):257–279, 2005.

[19] John Heidemann, Wei Ye, Jack Wills, Affan Syed, and Yuan Li. Research challenges and applications for underwater sensor networking. In *Proceedings of the IEEE Wireless Communications and Networking Conference (WCNC)*, volume 1, pages 228–235. IEEE, April 2006.

[20] Todd R. Martz, James G. Connery, and Kenneth S. Johnson. Testing the honeywell durafet® for seawater ph applications. *Limnology and Oceanography: Methods*, 8(5):172–184, 2010.

[21] Philip J. Bresnahan Jr, Todd R. Martz, Yuichiro Takeshita, Kenneth S. Johnson, and Michael LaShomb. Best practices for autonomous measurement of seawater ph with the honeywell durafet. *Methods in Oceanography*, 9:44–60, 2014.

[22] Taylor Wirth and et al. Assessment of a ph optode for oceanographic moored and profiling applications. *Limnology and Oceanography: Methods*, 22(11):805–822, 2024.

[23] Ingo Klimant, Volker Meyer, and Michael Kühl. Optical measurement of oxygen and temperature in microscale: Strategies and biological applications. *Sensors and Actuators B: Chemical*, 38(1–3):29–37, 1997.

[24] Dong Xu, Rui Xue, Ming Luo, Wei Wang, Wei Zhang, and Yong Wang. Advances in dissolved organic carbon remote sensing inversion in inland waters: Methodologies, challenges, and future directions. *Sustainability*, 17(14):6652, 2025.

[25] James D. Sharp, Brian N. Seegers, and Nicholas Briggs. Characterizing non-photochemical quenching in fluorometric chlorophyll sensors under variable light and temperature conditions. *Limnology and Oceanography: Methods*, 22(1):89–102, 2024.

[26] Catherine Mitchell and et al. A chlorophyll a, non-photochemical fluorescence quenching correction method for autonomous underwater vehicles in shelf sea environments. *Limnology and Oceanography: Methods*, 22(3):149–158, 2024.

[27] Thomas Pfeiffer, Malte Briese, and Peter Holtermann. Quality control and integration of multiparameter probes for autonomous marine observation platforms. *Ocean Science*, 14(6):1573–1589, 2018.

[28] Mohammad Furqan Ali et al. Recent advances and future directions on underwater wireless communications. *Archives of Computational Methods in Engineering*, 27(5), 2020.

[29] Mandar Chitre, Saeed Shahabudeen, and Milica Stojanovic. Underwater acoustic communications and networking: Recent advances and future challenges. *Marine Technology Society Journal*, 42(1):103–116, 2008.

[30] Pejman Panahi, Kourosh Ramezanpour, R. Javidan, Ali Dehghantanha, and Reza M. Parizi. Performance evaluation of lightweight encryption algorithms for iot-based applications. *Arabian Journal for Science and Engineering*, 46(4):4015–4037, 2021.

[31] Robert J. Urick. *Principles of Underwater Sound*. McGraw-Hill, 1983.

[32] Xavier Lurton. *An Introduction to Underwater Acoustics: Principles and Applications*. Springer, 2002.

[33] Daniel B. Kilfoyle and Arthur B. Baggeroer. The state of the art in underwater acoustic telemetry. *IEEE Journal of Oceanic Engineering*, 25(1):4–27, 2000.

[34] Ian F. Akyildiz, Dario Pompili, and Tommaso Melodia. Underwater acoustic sensor networks: Research challenges. *Ad Hoc Networks*, 3(3):257–279, 2005.

[35] Hemani Kaushal and Georges Kaddoum. Underwater optical wireless communication. *IEEE Access*, 4:1518–1547, 2016.

[36] Pawan Kumar, Shashank Jha, and Ritik Kumar Singh. Internet of underwater things (iout): A systematic review research. *Journal of Recent Innovations in Computer Science and Technology*, 2(1):28–47, 2025.

[37] Dario Pompili, Tommaso Melodia, and Ian F. Akyildiz. Three-dimensional and two-dimensional deployment analysis for underwater acoustic sensor networks. *Ad Hoc Networks*, 7(4):778–790, 2009.

[38] Gang Han, Jia Jiang, Chenyu Zhang, and Mohsen Guizani. A survey on mobile anchor node-assisted localization in underwater wireless sensor networks. *IEEE Communications Surveys & Tutorials*, 21(2):1608–1632, 2019.

[39] Shengming Jiang. On securing underwater acoustic networks: A survey. *IEEE Communications Surveys & Tutorials*, 21(1):729–752, 2018.

[40] Rudra Pratap Singh, Bhan Singh, and Navneet Kaur Popli. Temporal analysis of oceanographic data: Insights into environmental variability and trends. In *Proceedings of the 2024 IEEE Pacific Rim Conference on Communications, Computers and Signal Processing (PACRIM)*, pages 1–9, 2024.

[41] Mansahaj Singh Popli, Rudra Pratap Singh, Navneet Kaur Popli, and Mohammad Mamun. A federated learning framework for enhanced data security and cyber intrusion detection in distributed network of underwater drones. *IEEE Access*, 13:12634–12646, 2025.

[42] Robert D. Blevins. *Applied Fluid Dynamics Handbook*. Krieger Publishing, 2010.

[43] Kenneth V. Mackenzie. Nine-term equation for sound speed in the oceans. *The Journal of the Acoustical Society of America*, 70(3):807–812, 1981.

[44] Fernanda Henderikx Freitas and Heidi M. Dierssen. Evaluating the seasonal and decadal performance of red band difference algorithms for chlorophyll

in an optically complex estuary with winter and summer blooms. *Remote Sensing of Environment*, 231:111228, September 2019.

[45] E. J. Sylak-Glassman, J. Zaks, K. Amarnath, and et al. Characterizing non-photochemical quenching in leaves through fluorescence lifetime snapshots. *Photosynthesis Research*, 127:69–76, 2016.

[46] Abbas Jamalipour and Sarumathi Murali. A taxonomy of machine-learning-based intrusion detection systems for the internet of things: A survey. *IEEE Internet of Things Journal*, 9(12):9444–9466, 2021.

[47] Samir Ifzarne, Hiba Tabbaa, Hafidi Imad, and Nidal Lamghari. Anomaly detection using machine learning techniques in wireless sensor networks. *Journal of Physics: Conference Series*, 1743(1):012021, 2021. CC BY 3.0 License.

[48] Keith Bonawitz, Hubert Eichner, Wolfgang Grieskamp, et al. Towards federated learning at scale: System design. In *Proceedings of Machine Learning and Systems (MLSys)*, 2019. arXiv:1902.01046.

[49] Peter Kairouz, H. Brendan McMahan, et al. Advances and open problems in federated learning. *Foundations and Trends in Machine Learning*, 14(1–2):1–210, 2021.

[50] Wei Yang Bryan Lim, Nguyen Cong Luong, Duc Tien Hoang, et al. Federated learning in mobile edge networks: A comprehensive survey. *IEEE Communications Surveys & Tutorials*, 22(3):2031–2063, 2020.

[51] MDPI Sensors Editorial Board. Integrated ocean observation system schematic (fig. 1). *Sensors*, 19(1255), 2019.

[52] Mari Carmen Domingo. An overview of the internet of underwater things. *Journal of Network and Computer Applications*, 35(6):1879–1890, 2012.

[53] S. A. H. Mohsan, A. Mazinani, N. Q. H. Othman, and H. Amjad. Towards the internet of underwater things: A comprehensive survey. *Earth Science Informatics*, 15(2):735–764, 2022.

[54] Z. Zhu, Y. Zhou, R. Wang, and F. Tong. Internet of underwater things infrastructure: A shared underwater acoustic communication layer scheme for

real-world underwater acoustic experiments. *IEEE Transactions on Aerospace and Electronic Systems*, 59(5):6991–7003, 2023.

[55] M. Jahanbakht, W. Xiang, L. Hanzo, and M. R. Azghadi. Internet of underwater things and big marine data analytics—a comprehensive survey. *IEEE Communications Surveys & Tutorials*, 23(2):904–956, 2021.

[56] Tie Qiu, Zhao Zhao, Tong Zhang, Chen Chen, and C. L. Philip Chen. Underwater internet of things in smart ocean: System architecture and open issues. *IEEE Transactions on Industrial Informatics*, 16(7):4297–4307, 2019.

[57] K. M. Delphin Raj, Jinyoung Lee, Eunbi Ko, Soo-Young Shin, Jung-Il Namgung, Sun-Ho Yum, and Soo-Hyun Park. Underwater network management system in internet of underwater things: Open challenges, benefits, and feasible solution. *Electronics*, 9(7):1142, 2020.

[58] Shusen Jing, Joseph Hall, Yahong Rosa Zheng, and Chengshan Xiao. Signal detection for underwater iot devices with long and sparse channels. *IEEE Internet of Things Journal*, 7(8):6664–6675, 2020.

[59] A. A. Sheikh, E. Felemban, and A. Ashraf. Coralcon: An open source low-cost modem for underwater iot applications. In *Proceedings of the 2017 13th IEEE International Conference on Intelligent Computer Communication and Processing (ICCP)*, pages 503–508. IEEE, 2017.

[60] S. Kim, J. Y. Cho, D. H. Jeon, W. Hwang, Y. Song, S. Y. Jeong, and T. H. Sung. Propeller-based underwater piezoelectric energy harvesting system for an autonomous iot sensor system. *Journal of the Korean Physical Society*, 76(3):251–256, 2020.

[61] D. Wei, L. Yan, C. Huang, J. Wang, J. Chen, M. Pan, and Y. Fang. Dynamic magnetic induction wireless communications for autonomous-underwater-vehicle-assisted underwater iot. *IEEE Internet of Things Journal*, 7(10):9834–9845, 2020.

[62] I. Bayusari, N. A. Adawiyyah, S. Dwijayanti, H. Hikmarika, Z. Husin, and B. Y. Suprapto. Water quality monitoring system in autonomous underwater vehicle based on internet of things (iot). In *Proceedings of the 2021*

8th International Conference on Electrical Engineering, Computer Science and Informatics (EECSI), pages 328–334. IEEE, 2021.

[63] M. Salhaoui, J. C. Molina-Molina, A. Guerrero-Gonzalez, M. Arioua, and F. J. Ortiz. Autonomous underwater monitoring system for detecting life on the seabed by means of computer vision cloud services. *Remote Sensing*, 12(12):1981, 2020.

[64] Y. Harold Robinson, S. Vimal, E. Golden Julie, Manju Khari, Christopher Expósito-Izquierdo, and Javier Martínez. Hybrid optimization routing management for autonomous underwater vehicle in the internet of underwater things. *Earth Science Informatics*, 14(1):441–456, 2021.

[65] Jie Zhang, Jianfa Sha, Guangjie Han, Jun Liu, and Yujie Qian. A cooperative-control-based underwater target escorting mechanism with multiple autonomous underwater vehicles for underwater internet of things. *IEEE Internet of Things Journal*, 8(6):4403–4416, 2020.

[66] Syed Agha Hassnain Mohsan, Yanlong Li, Muhammad Sadiq, Junwei Liang, and Muhammad Asghar Khan. Recent advances, future trends, applications and challenges of internet of underwater things (iout): A comprehensive review. *Journal of Marine Science and Engineering*, 11(1):124, 2023.

[67] Tomas Higareda-Pliego, N. A. Adawiyyah, S. Dwijayanti, H. Hikmarika, Z. Husin, and B. Y. Suprapto. Design of a semi-autonomous iot submarine drone for the exploration and monitoring of hydraulic systems. *Pädi Boletín Científico de Ciencias Básicas e Ingenierías del ICBI*, 10:48–52, 2022.

[68] A. Hussain, S. Li, T. Hussain, R. W. Attar, A. Alhomoud, R. Alsagri, and K. Zaman. Energy-efficient and trust-based autonomous underwater vehicle scheme for 6g-enabled internet of underwater things. *Sensors*, 25(1):286, 2025.

[69] Antonio Vasilijević, đula Nađ, and Nikola Mišković. Autonomous surface vehicles as positioning and communications satellites for the marine operational environment—step toward internet of underwater things. In *Proceedings of the 2018 IEEE 8th International Conference on Underwater System Technology: Theory and Applications (USYS)*, pages 1–5. IEEE, 2018.

[70] F. Amador-Castro, T. García-Cayuela, H. S. Alper, V. Rodriguez-Martinez, and D. Carrillo-Nieves. Valorization of pelagic sargassum biomass into sustainable applications: Current trends and challenges. *Journal of Environmental Management*, 283:112013, 2021.

[71] T. B. Atwood, A. Witt, J. Mayorga, E. Hammill, and E. Sala. Global patterns in marine sediment carbon stocks. *Frontiers in Marine Science*, 7:165, 2020.

[72] L. T. Bach, P. Stange, J. Taucher, E. P. Achterberg, M. Algueró-Muñiz, H. Horn, et al. The influence of plankton community structure on sinking velocity and remineralization rate of marine aggregates. *Global Biogeochemical Cycles*, 33(8):971–994, 2019.

[73] L. T. Bach, V. Tamsitt, J. Gower, C. L. Hurd, J. A. Raven, and W. Boyd. Testing the climate intervention potential of ocean afforestation using the great atlantic sargassum belt. *Nature Communications*, 12:2556, 2021.

[74] M. Barange, M. Butenschön, A. Yool, N. Beaumont, J. A. Fernandes, A. P. Martin, et al. The cost of reducing the north atlantic ocean biological carbon pump. *Frontiers in Marine Science*, 3:290, 2017.

[75] M. Barbesgaard. Blue growth: Savior or ocean grabbing? *Journal of Peasant Studies*, 45(1):130–149, 2018.

[76] D. K. Barnes, C. J. Sands, A. Cook, F. Howard, A. R. Gonzalez, C. Muñoz-Ramirez, et al. Blue carbon gains from glacial retreat along antarctic fjords: What should we expect? *Global Change Biology*, 26:2750–2755, 2020.

[77] D. K. Barnes and G. A. Tarling. Polar oceans in a changing climate. *Current Biology*, 27(9):R454–R460, 2017.

[78] K. S. Bawa, N. Nawn, R. Chellam, J. Krishnaswamy, V. Mathur, S. B. Olsson, et al. Opinion: Envisioning a biodiversity science for sustaining human well-being. *Proceedings of the National Academy of Sciences (PNAS)*, 117(43):25951–25955, 2020.

[79] N. Bax, C. J. Sands, B. Gogarty, R. V. Downey, C. V. Moreau, B. Moreno, et al. Perspective: Increasing blue carbon around antarctica is an ecosystem service of considerable societal and economic value worth protecting. *Global Change Biology*, 27:5–12, 2020.

[80] E. Bayraktarov, M. I. Saunders, S. Abdullah, M. Mills, J. Beher, H. P. Possingham, et al. The cost and feasibility of marine coastal restoration. *Ecological Applications*, 26(4):1055–1074, 2016.

[81] N. Ahmed, S. W. Bunting, M. Glaser, M. S. Flaherty, and J. S. Diana. Can greening of aquaculture sequester blue carbon? *Ambio*, 46:468–477, 2017.

[82] T. V. Armentano and G. M. Woodwell. Sedimentation rates in a long island marsh determined by ^{210}Pb dating. *Limnology and Oceanography*, 20:452–456, 1975.

[83] D. Baldocchi, E. Falge, L. Gu, R. Olson, D. Hollinger, S. Running, et al. Fluxnet: A new tool to study the temporal and spatial variability of ecosystem-scale carbon dioxide, water vapor, and energy flux densities. *Bulletin of the American Meteorological Society*, 82:2415–2434, 2001.

[84] E. Q. Brannon, S. M. Moseman-Valtierra, C. W. Rella, R. M. Martin, X. Chen, and J. Tang. Evaluation of laser-based spectrometers for greenhouse gas flux measurements in coastal marshes. *Limnology and Oceanography: Methods*, 14:466–476, 2016.

[85] H. Charles and J. S. Dukes. Effects of warming and altered precipitation on plant and nutrient dynamics of a new england salt marsh. *Ecological Applications*, 19:1758–1773, 2009.

[86] X. C. Chen, W. Q. Dai, C. J. Huang, L. P. Pan, W. Wu, and W. H. You. Design of compound ecological purification system for preserving water quality of shanghai yingwuzhou wetland (in chinese). *China Water and Wastewater*, 33:66–70, 2017.

[87] X. C. Chen, R. F. Gao, and J. W. Tang. Basic views and technological methods of salt marsh restoration and its progress in implementation (in chinese). *Marine Environmental Science*, 35(3):1–18, 2016.

[88] J. L. Davis, C. A. Currin, C. O'Brien, C. Raffenburg, and A. Davis. Living shorelines: Coastal resilience with a blue carbon benefit. *PLOS ONE*, 10(11):e0142595, 2015.

[89] E. A. Davidson, K. Savage, L. V. Verchot, and R. Navarro. Minimizing artifacts and biases in chamber-based measurements of soil respiration. *Agricultural and Forest Meteorology*, 113:21–37, 2002.

[90] L. A. Deegan, D. S. Johnson, R. S. Warren, B. J. Peterson, J. W. Fleeger, S. Fagherazzi, and W. M. Wollheim. Coastal eutrophication as a driver of salt marsh loss. *Nature*, 490:388–392, 2012.

[91] D. C. Donato, J. B. Kauffman, D. Murdiyarso, S. Kurnianto, M. Stidham, and M. Kanninen. Mangroves among the most carbon-rich forests in the tropics. *Nature Geoscience*, 4:293–297, 2011.

[92] C. M. Duarte, I. J. Losada, I. E. Hendriks, I. Mazarrasa, and N. Marbà. The role of coastal plant communities for climate change mitigation and adaptation. *Nature Climate Change*, 3:961–968, 2013.

[93] C. B. Field, M. J. Behrenfeld, J. T. Randerson, and P. Falkowski. Primary production of the biosphere: Integrating terrestrial and oceanic components. *Science*, 281:237–240, 1998.

[94] Y. P. Gao, J. G. Fang, W. Tang, J. H. Zhang, L. H. Reng, and M. R. Du. Seagrass meadow carbon sink and amplification of the carbon sink for eelgrass bed in sanggou bay (in chinese). *Progress in Fishery Science*, 1:17–21, 2013.

[95] National Intelligence Council. Disruptive civil technologies: Six technologies with potential impacts on u.s. interests out to 2025. In *Conference Report CR*, 2008.

[96] Luigi Atzori, Antonio Iera, and Giacomo Morabito. The internet of things: A survey. *Computer Networks*, 54(15):2787–2805, 2010.

[97] Ari Juels. Rfid security and privacy: A research survey. *IEEE Journal on Selected Areas in Communications*, 24(2):381–394, 2006.

[98] Jean-Philippe Vasseur and Adam Dunkels. *Interconnecting Smart Objects with IP: The Next Internet*. Morgan Kaufmann, 2010.

[99] Jonathan Hui, David Culler, and Samita Chakrabarti. 6lowpan: Incorporating ieee 802.15.4 into the ip architecture—internet protocol for smart

objects (ipso) alliance white paper #3. Technical report, IPSO Alliance, 2009.

[100] Adam Dunkels and Jean-Philippe Vasseur. Ip for smart objects—internet protocol for smart objects (ipso) alliance white paper #1. Technical report, IPSO Alliance, 2008.

[101] Miodrag Potkonjak, Seap Meguerdichian, and Jonathan L. Wong. Trusted sensors and remote sensing. In *Proceedings of the IEEE Sensors Conference*, pages 1104–1107, 2010.

[102] Jun-Hui Kong, Lay-Ming Ang, and Kah-Phon Seng. Minimalist security and privacy schemes based on enhanced aes for integrated wisp sensor networks. *Journal of Communication Networks and Distributed Systems*, 11(2):214–232, 2013.

[103] Andrew M. Dunn et al. Eternal sunshine of the spotless machine: Protecting privacy with ephemeral channels. In *Proceedings of the 10th USENIX Symposium on Operating Systems Design and Implementation (OSDI)*, pages 61–75, 2012.

[104] Y. Tang. Cleanos: Limiting mobile data exposure with idle eviction. In *Proceedings of the 10th USENIX Symposium on Operating Systems Design and Implementation (OSDI)*, volume 12, pages 77–91, 2012.

[105] Edith Brown Weiss. United nations conference on environment and development. *International Legal Materials*, 31:814–817, 1992.

[106] Md Whaiduzzaman, Antonio Barros, M. Chanda, S. Barman, T. Sultana, M. S. Rahman, S. Roy, and C. Fidge. A review of emerging technologies for iot-based smart cities. *Sensors*, 22(23):9271, 2022.

[107] S. Deepaisarn, P. Yiwsiw, S. Chaisawat, T. Lerttomolsakul, L. Cheewakriengkrai, C. Tantiwattanapaibul, S. Buaruk, and V. Sornlertlamvanich. Automated street light adjustment system on campus with AI-assisted data analytics. *Sensors*, 23(3):1853, 2023.

[108] M. García-Castellano, J. M. González-Romo, J. A. Gómez-Galán, J. P. García-Martín, A. Torralba, and V. Pérez-Mira. ITERL: A wireless adaptive system for efficient road lighting. *Sensors*, 19(23):5101, 2019.

[109] C. C. Abarro, A. C. Caliwag, E. C. Valverde, W. Lim, and M. Maier. Implementation of IoT-based low-delay smart streetlight monitoring system. *IEEE Internet of Things Journal*, 9(18):18461–18469, 2022.

[110] C.-H. Liu, C.-Y. Hsiao, J.-C. Gu, K.-Y. Liu, S.-F. Yan, C. H. Chiu, and M. C. Ho. HCL control strategy for an adaptive roadway lighting distribution. *Applied Sciences*, 11(21):9960, 2021.

[111] O. O. Ordaz-García, M. Ortiz-López, F. J. Quiles-Latorre, J. G. Arceo-Olague, R. Solís-Robles, and F. J. Bellido-Outeiriño. DALI bridge FPGA-based implementation in a wireless sensor node for IoT street lighting applications. *Electronics*, 9(11):1803, 2020.

[112] G. Guerrero-Ulloa, A. Andrango-Catota, M. Abad-Alay, M. J. Hornos, and C. Rodríguez-Domínguez. Development and assessment of an indoor air quality control IoT-based system. *Electronics*, 12(3):608, 2023.

[113] J. Kim, J. Bang, A. Choi, H. J. Moon, and M. Sung. Estimation of occupancy using IoT sensors and a carbon dioxide-based machine learning model with ventilation system and differential pressure data. *Sensors*, 23(3):585, 2023.

[114] F. Rollo, C. Bachechi, and L. Po. Anomaly detection and repairing for improving air quality monitoring. *Sensors*, 23(3):640, 2023.